PERIODICO di MINERALOGIA
established in 1930

DIPARTIMENTO
DI SCIENZE DELLA TERRA

SAPIENZA
UNIVERSITÀ DI ROMA

An International Journal of
Mineralogy, Crystallography, Geochemistry,
Ore Deposits, Petrology, Volcanology
and applied topics on Environment, Archaeometry and Cultural Heritage

A preliminary petrographic and LA-ICP-MS trace elements study of the iron sulfide-rich deposits of Lombard Southern Alps: evidences of a hydrothermal origin?

Fabrizio Vergani

Department of Environmental Earth Sciences, University of Milano Bicocca, 20126 Milan, Italy

ARTICLE INFO

Submitted: May 2022
Accepted: September 2022
Available on line: September 2022

* Corresponding author:
fabrizio.vergani@unimib.it

Doi: 10.13133/2239-1002/17758

How to cite this article:
Vergani F. (2022)
Period. Mineral. 91, 201-224

ABSTRACT

Iron sulfide-rich deposits hosted in Middle Triassic to Early Jurassic limestones can be found in the Como Lake-Valsassina and Val Seriana areas (Southern Alps, Lombardy). These deposits were never studied in detail, other than a recent short publication about the petrography of the Piani d'Erna limonite deposit (Lecco). The aim of this paper is a preliminary study about these little-known sulfides deposits of the Lombard Southern Alps. These deposits were studied by field and petrographic investigations, SEM-EDS, LA-ICP-MS and XRPD analyses. The deposits of the Como Lake-Valsassina area are linked to the weathering of a Fe-Pb-Zn-Ba epigenetic low temperature mineralization. Their genesis seems to be linked to the migration of Fe-Pb-Zn-Ba-rich basinal fluids that seeped along strongly fractured portions of the Lower Triassic Esino Fm., with a possible genetic-link with the Resinelli Pb-Zn-Fe-Ba-F Alpine-type deposits. While the Val Seriana-West Iseo Lake area deposits are actually intensely weathered and possibly originate from primary hydrothermal pyrite-rich mineralization.

Keywords: Lombard Alps; sulfides; hydrothermal deposits; pyrite; marcasite; sphalerite; Alpine-type deposits; Pb-Zn deposits; Co/Ni ratios; LA-ICP-MS.

INTRODUCTION

Lombard southern Alps are rich in ore deposits exploited since antiquity, mainly siderite hydrothermal veins/stratabound bodies and Pb-Zn Alpine-type deposits. In the Como Lake-Valsassina (western Lombardy) and Val Seriana areas (eastern Lombardy) various iron sulfide-rich ore bodies can be found, hosted in Middle Triassic to Early Jurassic limestones. These deposits are usually deeply weathered and were exploited in the past mainly for limonite. Val Seriana deposits were never studied from a geological point of view, as a matter of fact most of these mining areas were rediscovered during the last few years. In a similar way, the Como Lake-Valsassina deposits were never studied in detail, the most recent work is a short publication (Ixer, 2006) about the petrography of Piani d'Erna limonite-rich deposit near Lecco, one of the deposits of Como Lake-Valsassina area. Ixer (2006) proposed an origin from deep weathering of a Fe-Pb-Zn-Ba hydrothermal epigenetic deposit for the Piani d'Erna ore body, possibly linked to the same mineralizing event of the Pian dei Resinelli Pb-Zn Alpine-type deposits.

Several Zn-Pb Alpine-type deposits are known in the Lombard Alps, in particular in the Gorno mining district. These deposits were very important for Zn and Pb production during the 19th and 20th centuries, with over 230 km of underground workings. These deposits comprise (a) Zn-Pb ores in the Gorno mining district (Omenetto, 1966); (b) dominant fluorite ores in the Paglio Pignolino-Dossena area (Jadoul and Omenetto 1980); (c) barite ores in the Brembana Valley; (d) fluorite-barite deposits, with subordinate Zn-Pb ores in the Presolana area (Jadoul and Omenetto 1980) and (e) Pb-Zn-barite ores in the Piani dei Resinelli-Como Lake area (Rodeghiero et al., 1986).

Alta Zinc Ltd. started in the last few years (2015) an

exploration program called "Gorno Zinc Project", with the aim of reopening the mines in the Gorno area. At the present day the new mining exploration of the Gorno Zn-Pb-Ag deposits identified 3.3 Mt of sulfides at 4.9% Zn, 1.3% Pb, and 27.2 g/t Ag. with also a mixed sulfides/non-sulfides mineralized body currently under evaluation (Mondillo et al., 2019). Moreover, in the last few years various new studies about the minerogenesis of the Gorno deposit were published (e.g. Mondillo et al., 2019; Giorno et al., 2021; Giorno et al., 2022), underlying the renewed scientific interest about the Lombard Zn-Pb Alpine-type deposits.

The aim of this paper is a preliminary study about the less-known deposits of Como Lake-Valsassina and Val Seriana areas, carried out by field and petrographic investigations, SEM-EDS, LA-ICP-MS and XRPD analyses. Minor and trace elements LA-ICP-MS analyses on sphalerite were carried out in order to study the possible roles of incorporation of trace elements within this sulfide and for preliminary thermometric evaluations, while LA-ICP-MS analyses on Fe-sulfides were carried out in order to discuss their Co/Ni ratios and their REE geochemistry.

This study, in particular, has the aim of evaluating the hypothesis proposed by Ixer (2006), about a possible connection between the studied deposits and the Lombard Pb-Zn Alpine-type deposits. The characterization of these deposits can, eventually, further improve the general knowledge about the Alpine-type deposits of Lombard Southern Alps.

GEOLOGICAL SETTING

A brief geological overview of the studied areas

Most Lombard ore deposits, those discussed in this paper included, are located to the South of the Insubric Line, in the South-Alpine domain of the Alps (Figure 1 a,b).

The Southern Alps are a south-verging thrust belt, separated from the north-verging, mainly metamorphic, Alps by the Insubric Line (Schmid et al., 1989).

The Lombard Southern Alps are divided into three stratigraphic portions separated by two major detachment structures (Berra and Felletti, 2006). The lower stratigraphic portion consists mainly of pre-Alpine basement units and basement-cored anticlines (known as Orobic anticlines), mostly made up of Permo-Carboniferous lithologies (Zanchetta et al., 2015). The southern limbs of the Orobic anticlines are overlain by Lower Triassic to Carnian prevailingly carbonate successions of the middle portion (Figure 1b). These carbonate successions are overlain by Jurassic and Cretaceous sedimentary rocks (upper

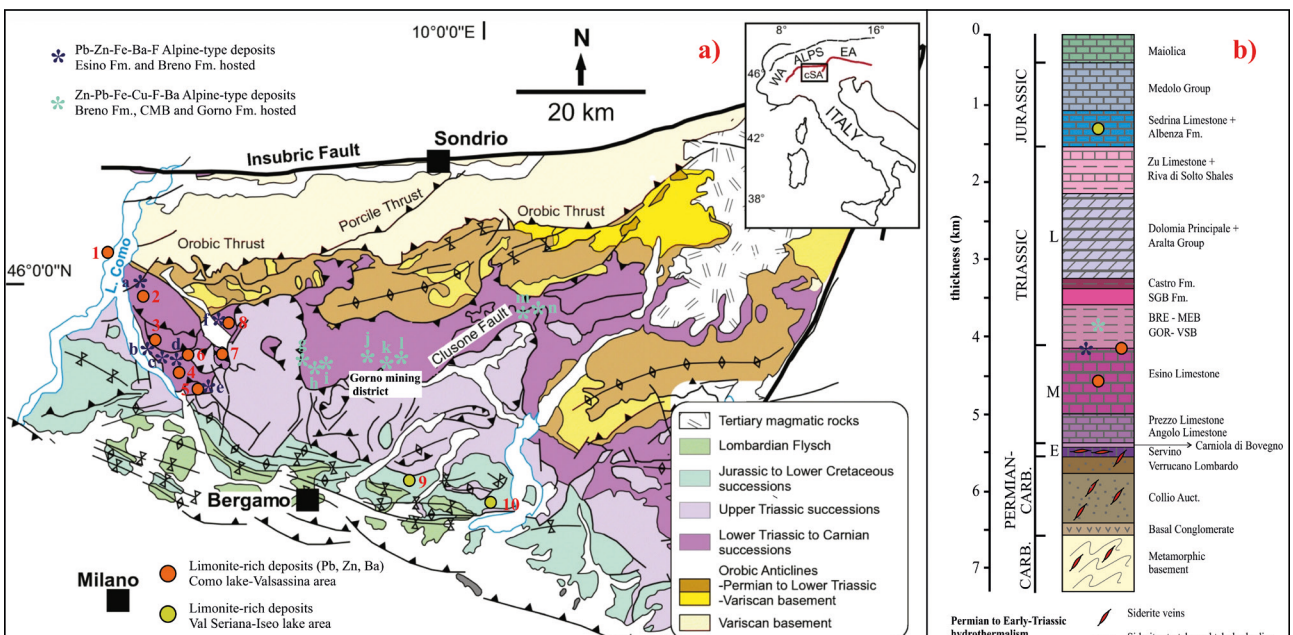

Figure 1. a) geological sketch map of the Lombard Southern Alps, the main limonite-rich and other limestone-hosted deposits are reported. b) Lithostratigraphic column of the Lombard Southern Alps, from Late Jurassic to Carboniferous. Modified from Zanchetta et al. (2015). E: Early, M: Middle, L: Late, CARB: Carboniferous. 1: Gaeta, 2: Esino Lario, 3: Mandello del Lario, 4: Ballabio, 5: Piani d'Erna, 6: Pasturo and Balisio, 7: Ferrera, 8: Campo del Ferro and Prato dell'Orso, 9: Büs del Fer, 10: Bronzone. a: Cubit Pb prospect, b: Mandello del Lario, c: Val Monastero, d: Pian dei Resinelli, e: Passata, g: Cespedosio, h: Paglio Pignolino, i: Mt.Vaccareggio, j: Mt. Arera, k: Val del Riso, l: Mt. Trevasco, m: Valzurio, n: Presolana (Polzone Lake).

portion) located in proximity of the Po plain (Zanchetta et al., 2015; Figure 1 a,b).

The ore deposits studied in this paper are located in the Como Lake-Valsassina area, western Lombardy, and in the Valseriana-West Iseo area in eastern Lombardy (Figure 1a). The deposits of western Lombardy are hosted by the Middle Triassic Esino Limestone in the middle stratigraphic portion of the Lombard Southern Alps (Figure 1b). Instead, the deposits in eastern Lombardy are hosted by the Early Jurassic Albenza Fm. and Sedrina Limestone, in the upper stratigraphic portion (Figure 1b).

The Esino Limestone (Ladinian) is a thick (up to 1000 m) carbonate platform dominated by shallow-water carbonates with a fast progradation in its upper part (Jadoul et al., 1992; Berra and Carminati, 2012). On the top of the Esino Formation palaeo-karsts, tepee horizons and a thin wedge of peritidal limestone, residual breccia bodies and terra-rossa deposits are observable, linked to.cyclical subaerial exposures (e.g., Berra, 2012; Vola and Jadoul, 2014). The Ladinian-Carnian boundary-related breccias at the top of the Esino platform host various Pb-Zn-Fe-Ba-F Alpine-type deposits (Pian dei Resinelli area; Rodeghiero et al., 1986). The contact between Esino Limestone and the underlying Bellano Fm. is sharp. The latter is characterized by fine-grained conglomerates with volcanic and metamorphic clasts, litarenites and hybrid dolostones (Sciunnach et al., 1996).

The Albenza Formation (Hettangian) is characterized by decimeter to meter-thick beds of light gray carbonates comprising sub-tidal to peritidal peloidal packstones interbedded with ooid-bioclastic grainstones (e.g., Jadoul and Galli, 2008). Its boundary with the overlying Sedrina Formation is usually sharp. The Sedrina Formation, up to 150 m thick (Bersezio et al., 1997), is formed by gray, open shelf, bioturbated mudstones, wacke-stones and peloidal packstones (Ronchi et al., 2011).

The limonite/Fe-Pb-Zn sulfide deposits of Lombard Alps

Most of the bibliography about the studied ore deposits belongs to the early 20th century and to the 19th century. Moreover, the deposits of eastern Lombardy were never studied from a geological point of view and most of them were rediscovered in the last few years.

The deposits of western Lombardy (Como Lake-Valsassina area) form veins, irregular bodies in pre-existing karst cavities and stockwork veins in heavily fractured parts of the host rock (Curioni, 1877; Repossi, 1904; Tizzoni, 1998).

These deposits are characterized by the presence of extensive gossans, exploited in the past for iron (limonite), with also common weathered iron sulfides as disseminations and/or nodules in the core zone of the deposits (Jervis, 1873; Curioni, 1877; Repossi, 1904; Tizzoni, 1998). Lead and zinc sulfides are also reported within the iron ores. The iron hydroxides may contain variable amounts of sulfur and metals (such as Pb, Zn, As and Sb), linked to the primary iron sulfides assemblage of each vein and to its degree of weathering. Frequently the vuggy iron hydroxides are mixed with variable amounts of lead-zinc secondary minerals, such as smithsonite, cerussite, anglesite and wulfenite (Repossi, 1904). The largest limonite-rich deposit of the area is located on the western shore of Como Lake, near Gaeta Cape (Jervis, 1873; Curioni, 1877; Repossi, 1904). It is characterized by large amounts of Pb and Zn sulfides, mainly in the deposit upper parts (Repossi, 1904).

FIELD STUDY OF THE COMO LAKE - VALSASSINA AND VALSERIANA - WEST ISEO DEPOSITS

Field studies were carried out on Gaeta, Piani d'Erna, Balisio, Ballabio, Barzio and Pasturo mines in the Como Lake-Valsassina area and on Büs del Fer and Mt. Bronzone mines in the Valseriana-West Iseo Lake area (Figure 1a).

The in-situ observations suggest for the Como Lake-Valsassina area deposits a limonite genesis linked to the weathering of a primary massive iron sulfides assemblage, with minor galena and sphalerite. In facts in these ore bodies unweathered parts of the ore deposit can be seen (Figure 2 a,b). They are dominated by massive fine-grained iron sulfides (pyrite and marcasite) and also by galena and sphalerite (Figure 2c). In general, these iron-rich Pb-Zn deposits seem to be stratabound and always linked to the dolomitized portions of Esino Fm. However, at the Gaeta mine some minor Pb-Zn sulfides bodies can be observed along the contact between the Esino Fm. basal member (ex Albigna Dolomite Fm.) and the underlying Bellano Fm (Figure 2d).

These deposits usually show a complex morphology and a wide range of geometry consisting of:

a) veins hosted by vertical faults with a E-W, N-S or NW-SE trend that crosscut Esino Fm. (Figure 2e);

b) fillings of pre-existing karst cavities, with complex geometries directly linked to those of the original karst cavities (e.g., Ballabio and Piani d'Erna mines, Valsassina area);

c) discordant stockwork veinlets along the host rock joint systems (Figure 2f);

d) sulfide-iron hydroxides-cemented dissolution and collapse breccias.

About the non-sulfide mineralization stage, possible iron sulfates and Zn-Pb-bearing secondary minerals are identifiable in the limonitic ore (Figure 2g). The gossan exhibits macroscopical textural features typical of supergene ores, with non-sulfides directly replacing sphalerite, galena and pyrite or present as concretions filling voids and cavities. Gypsum crystals were locally

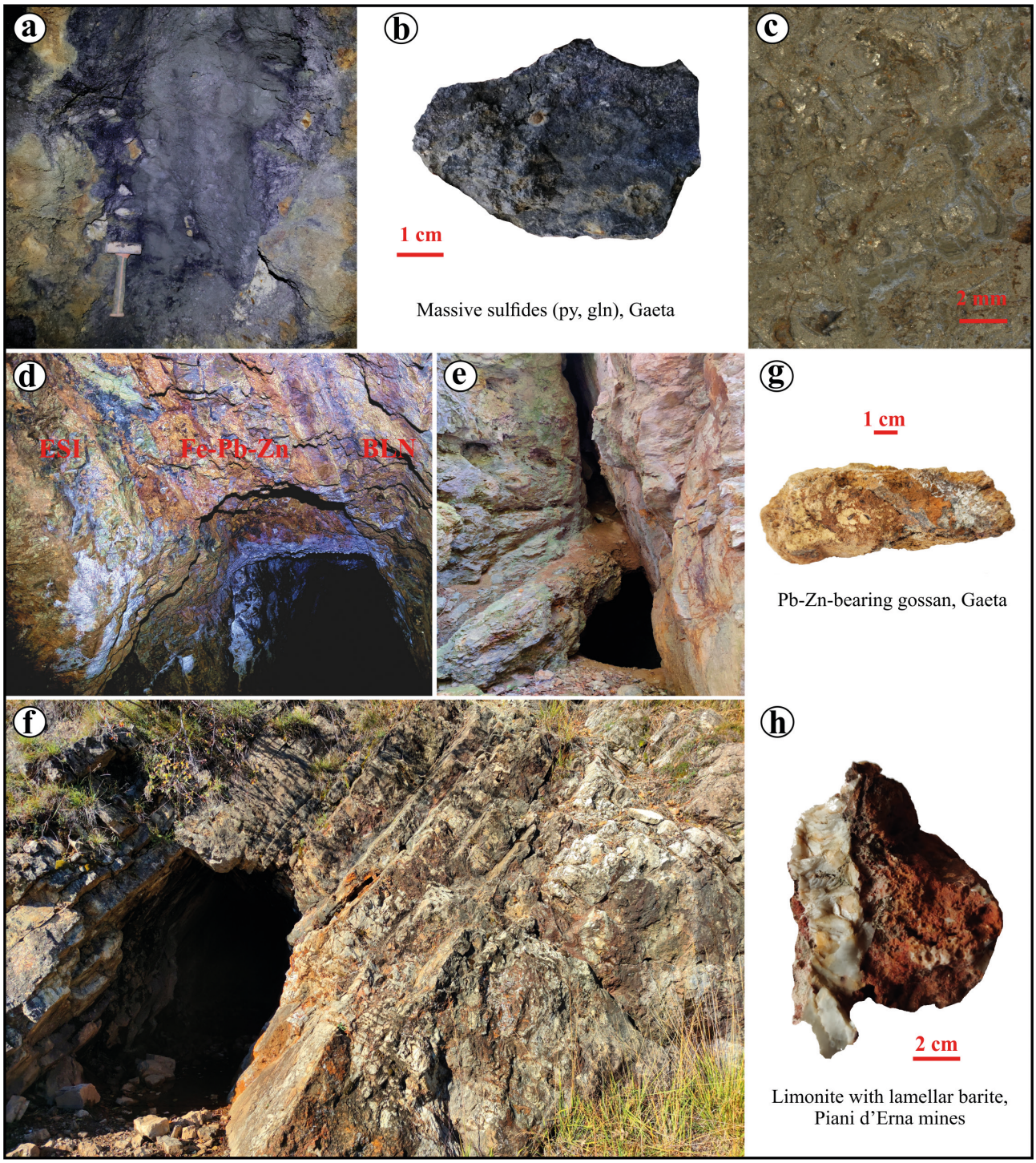

Figure 2. Como Lake-Valsassina pyrite-rich deposits. a) massive pyrite and marcasite vein, up to 1.5 m thick, from the innermost part of Pasturo mine, where its mineralization is less weathered; b) representative Pb-Zn-Fe sulfide ore sample, Gaeta mine; c) detail of a sample from Gaeta mine highest levels, galena and pyrite/marcasite with colloidal textures can be seen; d) galena-rich limonite ore bodies hosted within Esino Fm. at the contact with the underlying Bellano Fm., Gaeta mine highest levels; e) exploited fault-hosted vertical limonite/sulfides vein up to 40 cm thick, Pasturo mine; h) pyrite/marcasite and limonite-rich stockwork discordant veins near a prospection gallery, Gaeta mine highest levels; g) representative gossan ore sample with Pb-Zn non-sulfides, Gaeta mine; h) barite and limonite, Piani d'Erna mines.

observed within iron sulfate sinters in the old mines or as a gangue associated with weathered pyrite masses and other sulfides.

Barite is common in some deposits, like at Piani d'Erna mine and in the sulfide bodies at the Esino-Bellano Fm. contact, Gaeta mine (Figure 2h).

Val Seriana and West Iseo Lake deposits usually form strata-concordant tabular bodies, up to 1.5 m thick. Fine to coarse-grained weathered pyrite stockwork veinlets (with limonite pseudomorphs on pyrite euhedral crystals from 1 to 15 mm) hosted within the rock fractures are common (Figure 3a). They are associated with the main strata-concordant limonite bodies (Figure 3 b,d). Usually the limonite-rich ore shows banded and botryoidal textures, with minor carbonate (mainly calcite) gangue (Figure 3 e,f). Karst cavities are common in the mining areas crosscutting the limonite-rich beds. In the karst areas there are conglomerate bodies from lenticular to irregular in shape. These rocks include angular to rounded host rock, speleothems calcite/aragonite and limonite clasts within a micritic carbonate matrix (Figure 3g).

Sometimes limonite-pseudomorph on pyritized fossils, mainly bivalves, can be observed within the iron-rich samples. There are not sulfates or macroscopically detectable Pb-Zn bearing supergene phases in these ore deposits.

A detailed description of the various studied ore bodies is in the ESM.

PETROGRAPHIC OBSERVATIONS

Petrographic observations were made on polished samples from Gaeta, Pasturo, Piani d'Erna, Barzio, Büs del Fer and Mt. Bronzone mines. These observations are preliminary and may be incomplete because of the total loss of the primary ore textures in some of these deposits.

The primary mineralization process of the Como Lake-Valsassina deposits can be subdivided into three different ore stages, corresponding to their mineral assemblages and crosscutting relationships: early ore stage, late ore stage and supergene weathering stage. The minerals identified in these three ore stages are reported in Figure 5, along with their relative abundances.

Early ore stage (I): Como Lake-Valsassina deposits

As previously stated, in all the studied deposits the main ores are of secondary supergene origin. Nevertheless, in the upper and core zones of the Gaeta and Pasturo deposits the primary sulfide ore is far less weathered. Marcasite, pyrite, galena and sphalerite are dominant. Pyrite in all the samples from the Gaeta and Pasturo mines displays various textures, including: (a) fine grained pyrite with a grain size around 50 μm to 250 μm and variable shapes, from irregular to idiomorphic with mainly cubic habits; (b) irregular massive aggregates of pyrite; (c) rare framboidal pyrite and finally (d) pyritized microfossils. Disseminated pyrite can be found in the dolomitized host rocks, commonly as fine-grained disseminated crystals with cubic habitus (<0.5 mm), also associated with scattered granules of chalcopyrite and galena. However, in this ore stage the main metallic mineral is marcasite. It has mainly colloform textures with little blebs of galena and sphalerite as main inclusions, but it is also observable as fibrous aggregates after colloidal pyrite (Figure 4a). Fine-grained pyrite cubic crystals are at the border zones of colloidal marcasite and pyrite. Sphalerite and galena can be seen mainly inside the massive marcasite-pyrite ore (Figure 4b), in particular at the core of the marcasite colloidal masses. Often sphalerite shows colloidal textures around galena blebs. Zn and Pb sulfides are also present as little masses, veinlets and disseminations subsequent to the iron sulfide. Pyrite and marcasite are mostly weathered.

Late ore stage (II): Como Lake-Valsassina deposits

This ore stage is characterized by medium to coarse grained pyrite and common Pb-Zn sulfides (Figure 4c), usually associated with barite and dolomite as ore-filler. Barite forms lamellar crystals up to 2 mm and also scattered isolated lamellae. Pyrite is usually subordinate to Pb-Zn sulfides and it can be seen as irregular masses and granules up to 1 mm. Marcasite is rare. Galena is the main mineral in this ore stage and it can form big nodules and masses weighing up to many kg. It is common as inclusions within pyrite and sphalerite and also forms coarse-grained irregular masses and disseminated cubic crystals in barite gangue (Figure 4d). Pb-Sb and Pb-As sulfosalts (mainly boulangerite and gratonite) are relatively common as galena inclusions. Sphalerite is observable as irregular masses, granules and euhedral isolated crystals. This sulfide is usually moderately transparent and with honey-colored internal reflections.

In the upper portion of the Gaeta mine some minor mineralized bodies are reported along the contact between the Esino Fm. and the Bellano Conglomerate. The host arenaceous rocks show enrichment of fine-grained disseminated sulfides, mainly sphalerite and galena with minor pyrite (Figure 4e). Small scattered granules of chalcopyrite, cobaltite and arsenopyrite are locally widespread as small euhedral isolated crystals up to 0.2 mm, or as small masses formed by crystals aggregates.

Supergene weathering phase: Como Lake-Valsassina deposits

On the hand samples the limonite-rich ore (gossans) from Gaeta may change from massive red-brown to brown-yellow vuggy iron hydroxides with botryoidal and massive textures. Iron sulfates, such as jarosite, are

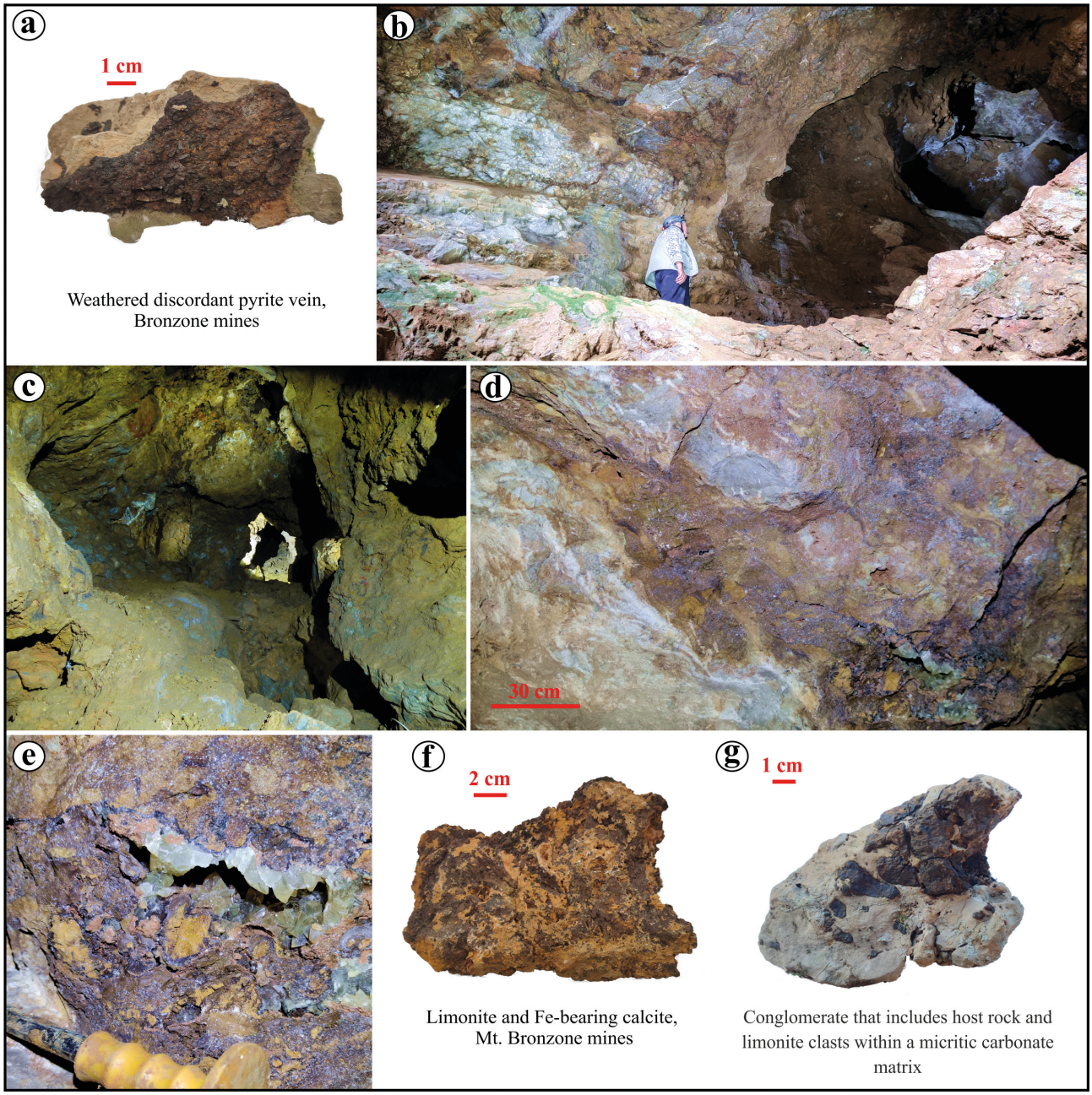

Figure 3. Valseriana-West Iseo Lake deposits. a) representative ore sample from Mt. Bronzone mines, limonite pseudomorph after pyrite; b) concordant to discordant limonite veins hosted by Albenza Fm. in one of the main stopes of Büs del Fer mine; c) exploitation works in a strata-concordant limonite mineralization up to 30 cm thick, Mt. Bronzone mines; d) a strata-concordant limonite mineralization up to 30 cm thick with calcite gangue, Mt. Bronzone mines; e) calcite cavity within massive limonite, Mt. Bronzone mines; f and g) representative sample from Mt. Bronzone mines.

common in the limonite, usually where there are weathered remains of pyrite and marcasite. Probably jarosite and other iron sulfates represent the intermediate weathering products of the iron sulfides. Gypsum and other sulfates can be found associated with microcrystalline marcasite weathered aggregates.

There are indeterminate manganese oxides/hydroxides as micro-aggregates of lamellar and acicular crystals inside the iron rich ore.

Traces of Pb and Zn carbonates such as cerussite and smithsonite are widespread in the limonite matrix, where there are also traces of other minerals such as anglesite

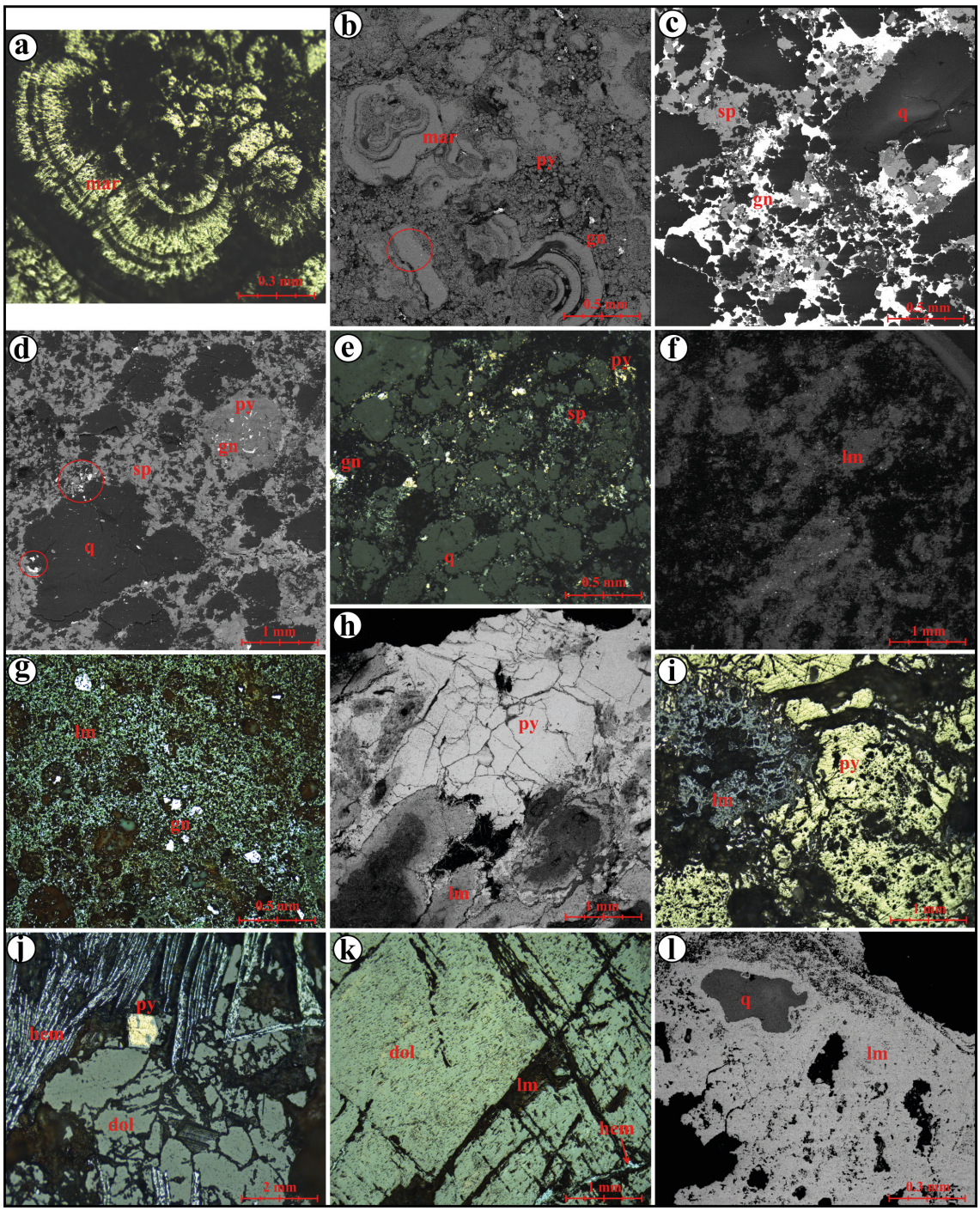

Figure 4. The textural and structural characteristics of sulfides, associated gangue minerals and iron-rich gossans viewed under SEM in BSE mode and reflected-light optical microscope. a) strongly weathered colloidal marcasite, Pasturo mine; b) colloidal marcasite with fine-grained pyrite, Pasturo mine, galena is also present in association to iron sulfides; c-d-e) Pb-Zn-Fe sulfides (± barite) present as substitution of the fine-grained matrix of the quartz arenaceous matrix (Bellano Fm., Gaeta mine); f) limonite from Gaeta mine lower levels shows common traces of Pb-bearing non-sulfides (white in BSE mode, mainly cerussite and anglesite); g) limonite from Gaeta mine higher levels commonly shows traces of residual galena; h-i) residual coarse-grained pyrite, Mt. Bronzone mines, in association to iron oxides/hydroxides (goethite and hematite); j) pyrite (partially substituted by limonite), dolomite and hematite, Mt. Bronzone mines; k) gangue Fe-rich dolomite with internal reflection partly substituted by iron hydroxides and hematite, Büs del Fer mine; l) quartz grain within limonite, Mt. Bronzone mines.. The mineral abbreviations are from Chace (1956). Sp: sphalerite, gn: galena, py: pyrite, mar: marcasite, lm: limonite, hem: hematite, q: quartz, dol: dolomite.

and wulfenite (Figure 4f). Smithsonite is also present as tiny rhombohedral crystals (up to 0.3 mm) in the limonite voids. Weathered galena remains are commonly observable within the gossan samples (Figure 4g).

Low reflectance, gray limonite occurs rarely as botryoidal bands, as irregular vuggy areas or as patches with a strong triangular cleavage. This suggests that it replaced a trigonal carbonate (dolomite/ankerite/siderite).

Ore stage: Val Seriana-West Iseo Lake deposits

The ore deposits of Val Seriana and West Iseo Lake area are characterized by the almost complete absence of sulfides, comprising mainly supergene minerals such as iron hydroxides. Pyrite and other iron minerals such as siderite and hematite, are present only as rare weathered remains within the limonitic ore. Pyrite is rare as coarse-grained granules, masses or as disseminated small crystals (up to 1 mm, Figure 4h). It is always strongly weathered and associated with an iron hydroxide alteration halo (Figure 4 h-j). Sporadic Fe-bearing calcite is present as weathered masses, with iron hydroxides along fractures and crystals boundaries (Figure 4k). Hematite form plumose aggregates of bladed crystals up to 5 mm, closely associated with Fe-bearing calcite, pyrite and goethite. The hematite crystals are usually corroded and partly transformed into iron hydroxides (Figure 4j).

Supergene weathering phase: Val Seriana-West Iseo Lake deposits

The limonitic ore in the Mt. Bronzone deposits show rhythmic and banded textures, pseudomorphs of cubic euhedral pyrite crystals with variable dimensions, often from 1 mm to 1.5 cm. Usually, they show rhythmic and banded textures as in compact limonite. Inside the limonitic ore there are sporadic lamellae of an indeterminate mineral of the clay group, hypothetically montmorillonite, and euhedral crystals of calcite. Quartz granules, up to 1 mm, are common within the limonitic ore (Figure 4l). Sometimes this calcium carbonate is associated also with iron hydroxides with banded textures. Often it forms white or gray crystals inside the cavities of limonite samples. Limonite masses with pronounced triangular cleavage, probably replacing a trigonal carbonate, such as dolomite/ankerite, siderite or calcite, are locally observable.

Minerals	Early ore stage	Late ore stage	Weathering stage
Pyrite	thin	bold	
Marcasite	bold	dashed	
Galena	thin	bold	
Sphalerite	dashed	bold	
Arsenopyrite		dashed	
Chalcopyrite		dashed	
Cobaltite		dashed	
Pb-As-Sb sulfosalts		dashed	
Gypsum		dashed	bold
Barite		bold	
Calcite	dashed	dashed	
Dolomite	dashed	dashed	
Iron hydroxides			bold
Cerussite			thin
Anglesite			dashed
Wulfenite			dashed
Smithsonite			dashed
Hemimorphite			dashed
Jarosite			thin

Figure 5. preliminary ore paragenesis of the Como Lake-Valsassina deposits. Bold lines: principal ore minerals, continuous lines: common accessory minerals, dashed lines: trace/sporadic minerals.

SAMPLING AND ANALYTICAL METHODS

Samples

The sampling strategy was planned on the basis of preliminary field observations. In particular, the sampling has interested the most representative deposits, where it was possible to collect samples suitable for the petrographic observations and/or the analytical studies.

Samples for petrographic observations and for polished sections preparation were collected in the Gaeta, Pasturo, Piani d'Erna, Barzio, Büs del Fer and Mt. Bronzone mines.

For the successive analytical investigations, samples from some of these localities were selected: Gaeta and Pasturo mines are the sites of the Como Lake-Valsassina area where the primary sulfide textures are best preserved, while the Mt. Bronzone mines are the only deposit in the Valseriana-West Iseo Lake area where non-weathered relics of the primary mineralization can be observed. Limonite samples for XRPD analysis were collected from the same localities. These samples were selected in order to avoid visually detectable Pb-Zn-bearing phases within limonite. XRPD analyses were also performed on representative samples of the secondary sulfates paragenesis of the Pasturo mine.

Finally, the LA-ICP-MS analyses were performed on sulfide samples collected from Gaeta and Mt. Bronzone mines, previously characterized during the petrographic observations. The samples from Pasturo mine were found far less suitable for the LA-ICP-MS analyses compared to the Gaeta and Mt. Bronzone samples.

LA-ICP-MS analyses were also performed on iron hydroxide samples from Gaeta and Mt. Bronzone mines. Two different limonite types were selected from Mt. Bronzone: black limonite pseudomorph on pyrite coarse-grained crystals and ochraceous laminated limonite.

A list of the studied samples is in Table 1.

SEM-EDS major element chemical analysis

Major elements analyses and SEM investigations were performed with a Tescan VEGA TS 5136XM equipped with an EDAX Genesis 4000 energy dispersive system

Table 1. summarizing table of the mining sites studied, samples and employed analytical techniques.

Mining site	Host rock	mineralization type	Samples description	n. samples	Analyses
Büs del Fer mine	Albenza Fm.	Val Seriana - West Iseo Lake	Banded gossan	5	SEM-EDS, petrographic observations
Bronzone mines	Sedrina Fm.	Val Seriana - West Iseo Lake	Massive gossan	7	SEM-EDS, petrographic observations
Bronzone mines	Albenza Fm.	Val Seriana - West Iseo Lake	Massive gossan	4	XRPD, SEM-EDS, ICP-LA-MS, petrographic observations
Bronzone mines	Albenza Fm.	Val Seriana - West Iseo Lake	Banded gossan (in paleo-karsic cavity)	3	XRPD, SEM-EDS, ICP-LA-MS, petrographic observations
Gaeta mine	Esino Fm.	Como Lake - Valsassina	Massive gossan	5	XRPD, SEM-EDS, ICP-LA-MS, petrographic observations
Gaeta mine	Esino Fm.	Como Lake - Valsassina	Gossan with Pb-Zn-bearing non-sulfides	3	SEM-EDS, petrographic observations
Gaeta mine	Esino/Bellano Fm.	Como Lake - Valsassina	Pb-Zn-Fe sulfides	6	SEM-EDS, ICP-LA-MS, petrographic observations
Gaeta mine	Esino Fm.	Como Lake - Valsassina	Sulfide nodules in the gossan	4	SEM-EDS, ICP-LA-MS, petrographic observations
Pasturo mine	Esino Fm.	Como Lake - Valsassina	Massive gossan	4	XRPD, SEM-EDS, petrographic observations
Pasturo mine	Esino Fm.	Como Lake - Valsassina	Secondary sulfates	2	XRPD, SEM-EDS
Pasturo mine	Esino Fm.	Como Lake - Valsassina	weathered massive sulfides	5	SEM-EDS, petrographic observations
Barzio mines	Esino Fm.	Como Lake - Valsassina	Gossan with Zn non-sulfides	3	SEM-EDS, petrographic observations
Erna mines	Esino Fm.	Como Lake - Valsassina	Massive gossan	3	SEM-EDS, petrographic observations

(EDS) at Milano Bicocca University. For the SEM-EDS semi-quantitative analyses certificated Astimex standards were used. SEM-EDS analyses were conducted on polished samples positioned on aluminum stubs carrying bi-adhesive carbon pads and either carbon coated. The latter was necessary to induce higher sample conductivity.

The scanning electron microscope was also used for the petrographic observations on polished samples, in addition to the reflected light optical microscope. In this way it was possible to study the textures of the various minerals in the ore samples as well as to determine their chemical composition by the means of the EDS microprobe. This is useful for those minerals whose determination by optical microscopy alone may be dubious.

X-Ray Powder Diffraction (XRPD)

Samples were grinded in agate mortar and back loaded into an Al sample holder. The XRPD study was conducted using a Bragg–PANalytical X'Pert-Pro PW3060 diffractometer with θ–θ geometry and CuKα radiation, in the 5-80° 2 range with step size of 0.02°, at room temperature and operating conditions of 40 mA and

40 kV. Qualitative phase analysis was carried out with the PANalytical X'Pert High Score software, using the ICSD PDF2-2004 database.

LA-ICP-MS minor and trace element chemical analysis

The LA-ICP-MS technique was used to analyze a wide range of trace elements in pyrite, marcasite, sphalerite and limonite samples (especially, Ge, Ga, In, Mn, Fe and Sn in sphalerite). The trace element analyses were carried out using a LA-ICP-MS at the GeoRessources laboratory (Vandoeuvre-lès-Nancy, France) composed of a 193 nm MicroLas Pro ArF Excimer coupled with the Agilent 7900 quadrupole ICP-MS.

Laser ablations were performed with a constant 5 Hz pulse rate, 60-micron spot size, at 6 J laser energy. The ablation duration for background, peaks and washouts was 30, 40 and 20 s respectively. The integration time was 20 ms for REE and 10 ms for the other elements. For REE higher integration time was selected in order to enhance the counts number. The ablated material was transported using a constant He flow (650 ml/min) and mixed with Ar in a cyclone coaxial mixer prior to entering the ICP torch and being ionized. The ions were successively sampled, accelerated and focused before being separated and analyzed in the quadrupole mass spectrometer. The following isotopes were monitored: ^{23}Na, ^{31}P, ^{39}K, ^{47}Ti, ^{51}V, ^{55}Mn, ^{57}Fe, ^{63}Cu, ^{66}Zn, ^{59}Co, ^{60}Ni, ^{71}Ga, ^{74}Ge, ^{75}As, ^{88}Sr, ^{89}Y, ^{95}Mo, ^{107}Ag, ^{111}Cd, ^{115}In, ^{118}Sn, and ^{121}Sb, ^{139}La, ^{140}Ce, ^{141}Pr, ^{146}Nd, ^{147}Sm, ^{153}Eu, ^{157}Gd, ^{159}Tb, ^{163}Dy, ^{165}Ho, ^{166}Er, ^{169}Tm, ^{172}Yb, ^{175}Lu, ^{182}W, ^{197}Au, ^{205}Tl, ^{208}Pb, ^{209}Bi, ^{232}Th and ^{238}U. For the limonite samples Na, P, K, Ti, V, Mn, Cu, Zn, Co, Ni, As, Sr, Y, Mo, Ag, Sb, REE, Au, Tl, Pb, Bi, Th and U were analyzed. Whereas Mn, Cu, Co, Ni, Ga, Ge, As, Y, Mo, Cd, In, Sn, Sb, REE, W and Bi were analyzed in sphalerite. Ti, V, Cu, Zn, Co, Ni, Y, Mo, Ag, Sb, REE, Au, Tl and Pb were analyzed in pyrite/marcasite. The analyses were calibrated with MASS-1 using the values published by Wilson et al. (2002), NIST610 and goethite OPB7 5-8 standards. The iron values obtained from SEM-EDS analyses were the internal standard for pyrite and limonite, while Zn was the internal standard for sphalerite.

Limit of detection (LOD) and uncertainty depends on the ablation spot diameter and the analyzed element. For each analysis, LOD was calculated using the 3σ criterion detailed in Longerich et al. (1996), uncertainty was calculated including the ones on the net transient signal (σ) and on the internal standard concentration. Minimum LOD were usually lower than 1 ppm for the trace elements analyzed at ablation 60 μm spot diameters.

For Ce and Eu anomalies evaluation the data were normalized to the Post-Archean Australian Shale values (PAAS, Taylor and McLennan, 2009), applying the following equations:

Table 2. XRPD analytical results. goe: goethite, lep: lepidocrocite, gyp: gypsum; jar: jarosite, fbr: fibroferrite, eps: epsomite, agl: anglesite, qtz: quartz; cal: calcite.

Sample id.	Location	Host rocks	Description	goe	lep	gyp	jar	fbr	eps	agl	qtz	cal
CB1	Pasturo mine	Esino Fm.	Massive gossan	59%	-	26%	15%	-	-	-	-	-
CB2	Pasturo mine	Esino Fm.	Secondary sulfates	-	16%	-	84%	-	-	-	-	-
CB3	Pasturo mine	Esino Fm.	Secondary sulfates	-	88%	-	12%	-	-	-	-	-
CB4	Pasturo mine	Esino Fm.	Secondary sulfates	-	43%	10%	15%	21%	11%	-	-	-
GAE1	Gaeta mine	Esino Fm.	Massive gossan	68%	-	12%	20%	-	-	-	-	-
GAE2	Gaeta mine	Esino Fm.	Massive gossan	59%	-	15%	21%	-	-	5%	-	-
BRZ1	Bronzone mines	Serina Fm.	Massive gossan	85%	-	-	-	-	-	-	15%	-
BRZ5	Bronzone mines	Albenza Fm.	Banded gossan	63%	13%	-	-	-	-	-	-	24%
BRZ6	Bronzone mines	Albenza Fm.	Banded gossan	76%	-	-	-	-	-	-	24%	-

$$\text{Log } (Ce/Ce^*) = \log Ce_N/(2 \log Pr_N - \log Nd_N)$$
$$\text{Log } (Eu/Eu^*) = \log Eu_N - (\log Gd^*_N + \log Sm_N)/2$$

RESULTS

XRPD determination of the secondary minerals

XRPD analyses were performed on representative samples of the secondary sulfates paragenesis of Pasturo mine and on limonite samples from Gaeta, Pasturo and Mt. Bronzone mines.

The secondary sulfate assemblages are formed by phases such as gypsum, fibroferrite, jarosite and anglesite (Table 4). Gypsum being the most widespread sulfate, usually it is the main mineral in the sulfate casts on the mine walls and in the weathered pyrite rich areas. While jarosite, gypsum, anglesite and other Pb-Zn-bearing supergene phases such as hemimorphite, smithsonite, cerussite and wulfenite are found in the gossan (see also chapter 4 - petrographic observations), fibroferrite and epsomite seem to be present only in the sulfate casts. Their formation is linked to sulfate-iron rich water percolating in the old mines.

All the limonite samples from Pasturo and Gaeta are jarosite and gypsum-bearing, suggesting that sulfates are commonly diffused in the gossan along with goethite. Instead, the samples from the West Iseo Lake area do not show any presence of sulfates and of Pb-Zn bearing phases. In general, they seem to be mainly iron hydroxides with only minor traces of quartz and calcite, minerals commonly crystallized within the limonite cavities, as reported during our field and petrographic observations.

Ore chemistry

Sphalerite:

The dataset includes 22 spot analyses in early-stage sphalerite and 11 in late-stage sphalerite from the Gaeta mine. The trace elements in Gaeta sphalerite from the two identified mineralization stages are summarized in Table 2 (complete analyses in table ESM 1).

The variations in representative elements are shown in Figure 6. In general, the concentrations of most of the analyzed trace elements in the sphalerite from the two hydrothermal stages changes considerably (e.g., Cd, Mn, Ge, Cu, Sb, In and Sn; Table 2).

Late-stage sphalerite shows more variable Zn values than early-stage sphalerite (Figure 6a), ranging from 60.55 to 63.43. In general, sphalerite displays significant Fe concentration in all spot analyses (Table 2; Figure 6a). The Fe contents in early and late-stage sphalerites are similar and range from 1.17 to 1.79 wt% and from 1.22 to 2.57 wt%, respectively. Early-stage sphalerite has lower concentrations of Ge, Ga, Cd, In, Sb and Sn than late-stage sphalerite (Figure 6 a-e). The concentrations of Ge, Ga, Cd, In and Sn in late-stage sphalerite range from 2.57 to 632 ppm, 426 to 4124 ppm, 6723 to 35185 ppm, 0.05-0.98 ppm, and 1.12 to 9.10 ppm, respectively. Cd is more concentrated in late than early sphalerite (Figure 6a) and shows a clear inverse correlation with Zn in the late-stage sphalerite (Figure 6b). Fe and Cd are probably present in the sphalerite lattice due to simple substitutions of Zn. On the other hand, direct correlations can be observed for Cu-Ge (Figure 6c), Cu-Ga (Figure 6d) and In-Sn (Figure 6e), suggesting that these elements are correlated with each other and are present in the sphalerite lattice due coupled substitutions of Zn.

Both early and late-stage sphalerite show Co concentrations (average 1.03 ppm and 3.43 ppm, respectively) higher than Ni (average 0.17 and 0.08, respectively). The concentrations of Mn are slightly higher in early than in late-stage sphalerite. In all spot analyses, Bi and Mo concentration is extremely low.

REE concentrations are generally under the detection limits, with only two spots analysis on early-stage sphalerite showing all the REE above the d.l.

Pyrite and marcasite:

The dataset includes 10 and 11 LA-ICP-MS spot analyses in early-stage marcasite and late-stage pyrite from Gaeta, respectively, and 9 spot analyses on pyrite from Mt. Bronzone mines. For the Gaeta deposit only late-stage pyrite was characterized. Early-stage pyrite is usually from weakly to strongly weathered and it was not possible to prepare samples suitable for LA-ICP-MS analyses. As previously discussed, micro-inclusions of Pb-Zn sulfides are present mainly within the marcasite, LA-ICP-MS spots were selected in order to avoid these inclusions. Table 2 shows pyrite and marcasite analyses (see also table ESM 2).

Co and Ni are minor components in pyrite and marcasite from the Gaeta and Mt. Bronzone deposits (Figure 7a). Mt. Bronzone pyrite shows higher Co/Ni values (between 0.23 and 6.70) if compared to Gaeta marcasite (0.01-0.07) and pyrite (0.02-5.60). Zn, Pb, Cu, As and Sb are important trace elements within marcasite and pyrite. Marcasite and pyrite from Gaeta are far more enriched in Zn and Pb if compared to Mt. Bronzone pyrite. Average values of 1350 ppm Zn and 2150 ppm Pb for Gaeta pyrite, 3800 ppm Zn and 2700 ppm Pb for Gaeta marcasite can be compared to 6 ppm Zn and 40 ppm Pb for Mt. Bronzone pyrite. Sb and Cu are in more variable amounts in Mt. Bronzone pyrite (Figure 7b), with higher average values in marcasite and pyrite from Gaeta. Both Gaeta and Mt. Bronzone marcasite and pyrite show a strong direct correlation between Sb and Cu (Figure 7b), with also a direct correlation between Sb and Zn (Figure 7c). This may suggest the presence of a Zn-Cu-Sb-bearing phase (e.g., tetrahedrite) in this pyrite. However, Zn in marcasite

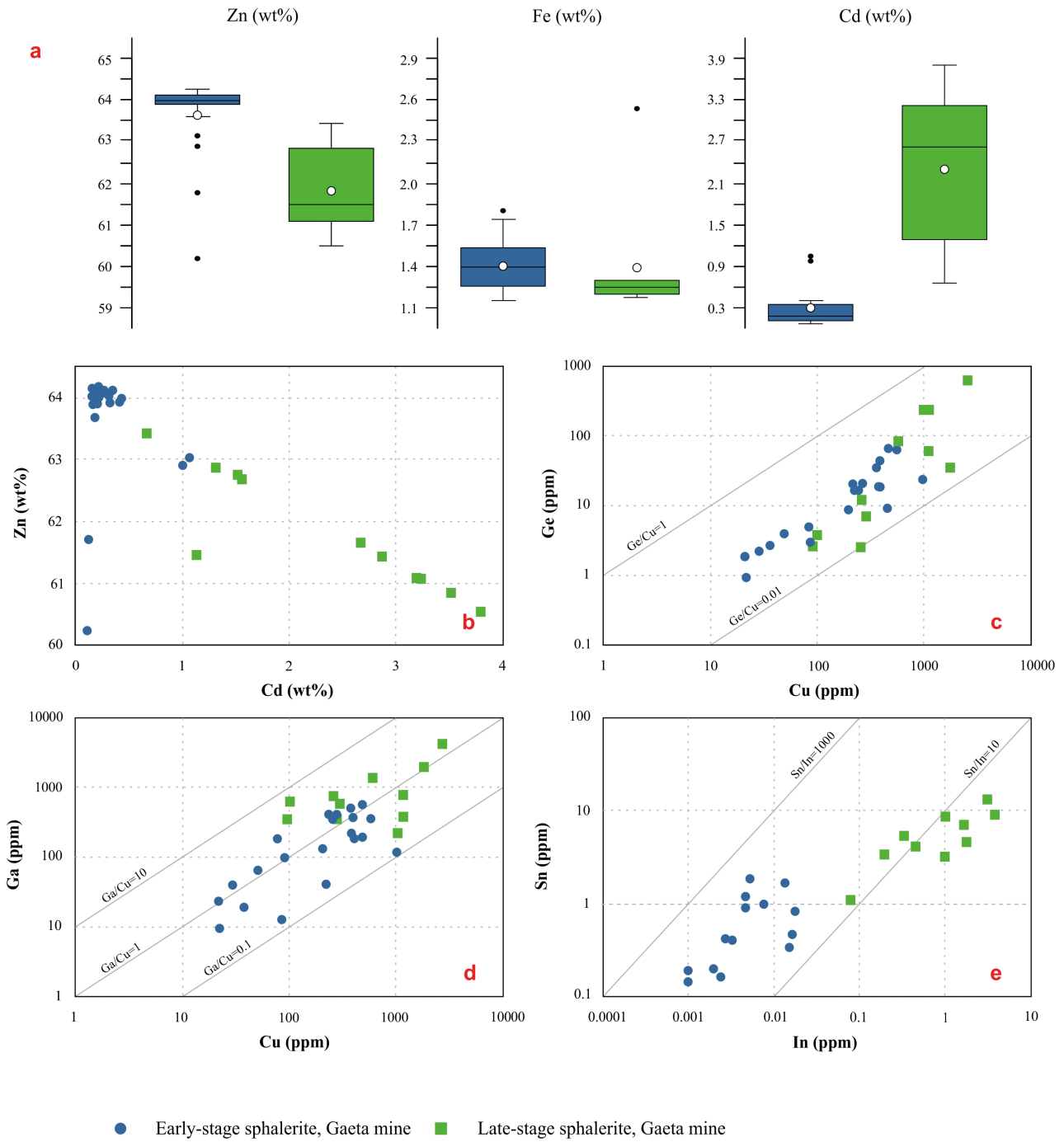

Figure 6. Major, minor and trace element plots of Gaeta sphalerite: a) statistical dispersion box-plots of Zn, Fe and Cd (for all the box plots, the coloured box contains 50% of the data, the white dot indicates the mean, the horizontal continuous line the median, while the black dots represent the outliers); b) Zn vs Cd; c) Ge vs Cu; d) Ga vs Cu and e) Sn vs In.

and pyrite from Gaeta is probably linked mainly to the presence of sphalerite nano-inclusions.

Ag and Mo are other important trace elements in marcasite and pyrite. Mo is averagely more enriched in Mt. Bronzone pyrite, with values over 1000 ppm, than in the marcasite and pyrite from Gaeta (Figure 7e). To the contrary, Ag is strongly enriched in Gaeta ore, its values ranging from 130 to 480 ppm and from 180 to 390 ppm for

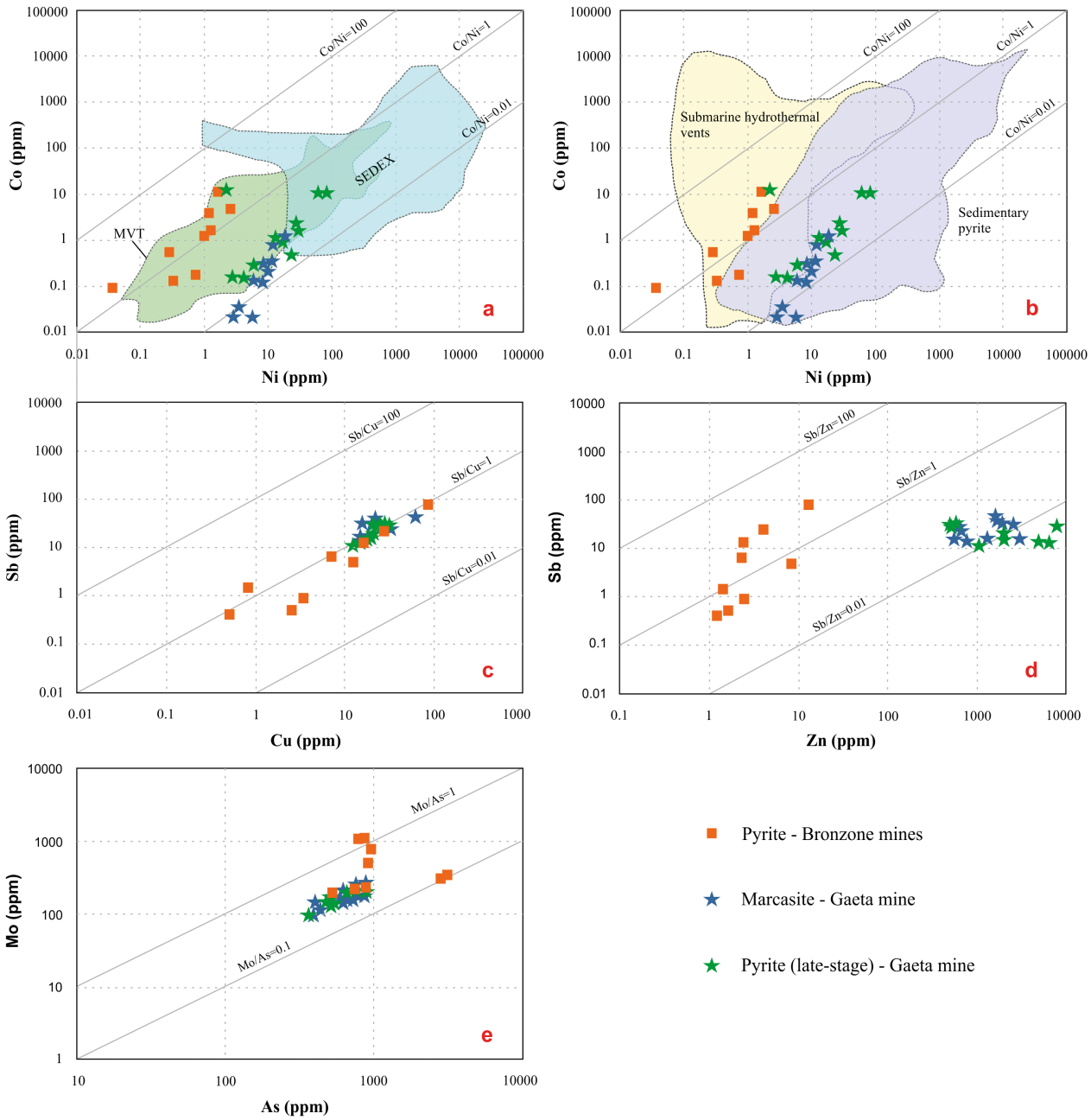

Figure 7. Trace element plots of Gaeta iron sulfides (pyrite and marcasite) and Mt. Bronzone pyrite: a,b) Co vs Ni; c) Sb vs Cu; d) Sb vs Zn and e) Mo vs As. Geochemical data for pyrite (Co/Ni ratios) from other deposits are displayed as colored fields: SEDEX (Howard's Pass district - Canada, McArthur Basin - Australia; Gadd et al., 2016; Mukherjee and Large, 2017), MVT deposits (Jinding, Hoshbulak and Qilinchang deposits, China; Li et al., 2015; Wang et al., 2018, Oyebamiji et al., 2020), sedimentary pyrite (Global; Berner et al., 2013; Large et al., 2014; Gregory et al., 2017; Mukherjee and Large, 2017) and submarine hydrothermal vents (Keith et al., 2016).

pyrite and marcasite (0.01-1.8 for Mt. Bronzone pyrite). Both pyrite and marcasite show a strong direct correlation between Ag and Sb, suggesting that silver is hosted in Sb-bearing nano-inclusions in iron sulfides.

Marcasite and pyrite from Gaeta are more Tl enriched (average 285 and 185 ppm respectively) if compared to Mt. Bronzone pyrite (average 36 ppm). Since Tl-bearing minerals have not been observed in these deposits, Tl is likely present as nanoparticles or as lattice substitutions in pyrite and marcasite. Gaeta marcasite is less enriched in Te

than pyrite from Gaeta and Mt. Bronzone, but this metal is always present in small amounts, with concentrations lesser than 10 ppm. Ti and V are more enriched in Gaeta pyrite and marcasite if compared to Mt. Bronzone pyrite.

Pyrite and marcasite from these mines have very low total REE contents (∑REE<1 ppm), with also values commonly under the detection limits. Gaeta pyrite and marcasite have a slightly positive Eu anomaly (Eu/Eu*) if normalized to the Post-Archean Australian Shale (PAAS), with average values of 1.27 and 1.48 respectively.

Limonitic ore:

The dataset comprises 11 LA-ICP-MS spot analyses on Bronzone limonite and 10 on Gaeta limonite. Table 3 shows the limonite analyses (complete analyses in table ESM 3).

Limonites from Como Lake-Valsassina area (Gaeta mine) and from Val Seriana-West Iseo Lake area show clear differences in their own trace element concentrations. The major element analyses of mixed limonite-rich non-sulfide ores are reported in table ESM 4.

Limonite from Gaeta is more enriched in Na (average 110 ppm) if compared to that from Mt. Bronzone (average 30 ppm for black limonite and 17 ppm for earthy limonite). Likewise, K is more enriched in Gaeta limonite (average

Table 3. Summarizing table of Mt. Bronzone pyrite and Gaeta pyrite, marcasite and sphalerite trace elements ICP-LA-MS analyses. For the complete analyses see the ESM. All the data are in ppm. For sphalerite the Fe and Zn (wt%) contents are also reported. Py: pyrite, Mar: marcasite, Sph-es: early-stage sphalerite, Sph-ls: late-stage sphalerite.

Sph-ls, Gaeta (11)	Zn	Fe	Cd	In	Mn	Ga	Ge	Sn	Cu	As
Min.	60.550	1.220	6722.691	0.080	0.563	217.148	2.575	1.123	93.831	0.647
Max.	63.430	2.570	37956.431	3.792	4.512	4124.918	631.923	31.223	2624.319	141.590
Average	61.818	1.393	23186.948	1.203	1.537	1027.366	172.947	8.341	844.132	28.623
Std deviation	0.962	0.394	10972.433	1.256	1.151	1143.103	210.170	8.315	802.107	41.351
d.l.	0.500	0.500	0.670	0.001	0.087	0.005	0.048	0.054	0.061	0.205
Sph-es, Gaeta (22)	Zn	Fe	Cd	In	Mn	Ga	Ge	Sn	Cu	As
Min.	60.240	1.170	1078.652	< d.l.	1.000	< d.l.	< d.l.	0.147	7.648	< d.l.
Max.	64.100	1.790	10737.932	0.018	16.598	549.909	66.175	80.347	996.739	36.815
Average	63.630	1.420	3030.075	0.007	3.146	191.784	19.256	4.187	264.212	8.003
Std deviation	0.940	0.180	2558.322	0.006	4.157	176.923	19.550	17.018	236.703	9.389
d.l.	0.500	0.500	0.429	0.001	0.462	0.002	0.053	0.045	0.07	0.214
Mar, Gaeta (10)	Zn	Pb	Cu	Co	Ni	Ag	Mo	As	Sb	Tl
Min.	502.179	1667.782	12.639	0.020	2.773	152.411	99.957	352.412	11.924	153.189
Max.	11701.892	4253.779	30.155	9.952	75.247	389.888	223.500	868.766	32.222	555.030
Average	3780.609	2707.632	21.251	1.303	15.282	234.792	171.032	580.211	22.891	287.322
Std deviation	3865.967	903.610	5.739	3.062	21.402	72.867	40.591	160.626	8.421	123.756
d.l.	0.657	0.049	0.077	0.004	0.122	0.001	0.001	0.252	0.010	0.003
Py, Gaeta (11)	Zn	Pb	Cu	Co	Ni	Ag	Mo	As	Sb	Tl
Min.	2.871	67.733	14.968	0.033	2.087	0.519	93.947	377.457	14.371	42.668
Max.	3049.743	3577.123	62.326	11.696	58.903	480.811	254.146	855.041	44.191	336.723
Average	1343.526	2151.494	23.733	2.582	16.328	208.172	171.541	624.638	25.229	185.335
Std deviation	929.087	846.949	14.233	4.164	17.161	116.163	49.338	169.819	10.110	84.418
d.l.	0.832	0.055	0.068	0.006	0.174	0.010	0.015	0.283	0.024	0.021
Py, Bronzone (9)	Zn	Pb	Cu	Co	Ni	Ag	Mo	As	Sb	Tl
Min.	1.278	1.574	0.514	0.089	0.034	0.016	193.286	510.139	0.422	12.342
Max.	13.584	217.197	84.802	10.669	2.422	1.821	1078.442	3056.699	77.249	109.431
Average	4.265	39.977	17.209	2.503	0.956	0.402	525.518	1268.050	14.384	36.395
Std deviation	4.173	69.139	26.819	3.450	0.744	0.593	360.205	948.447	24.853	33.835
d.l.	0.653	0.045	0.051	0.006	0.132	0.009	0.013	0.256	0.022	0.011

Table 4. summarizing table of Gaeta and Mt. Bronzone limonite trace elements ICP-LA-MS analyses. For the complete analyses see the ESM. All the data are in ppm. lm: limonite.

lm., Gaeta (11)	Zn	Pb	Cu	Ag	As	Sb	Tl	Mn	Mo	P	Na	K	Sr
Min.	7.577	13.286	120.794	11.055	536.798	14.637	2.812	16.044	52.630	108.189	48.278	85.112	1.395
Max.	2475.546	3112.578	144.226	2832.670	2783.295	1475.878	269.301	40.872	2098.188	266.859	222.742	4712.782	4.058
Average	1106.844	523.800	133.350	441.972	1805.746	412.465	47.692	23.662	697.979	150.329	110.089	1317.927	2.444
Std deviation	676.431	1072.632	8.597	819.823	709.556	591.065	89.762	7.661	812.073	57.135	68.230	1430.611	0.817
d.l.	0.407	0.016	0.044	0.001	0.181	0.019	0.017	0.685	0.002	6.818	0.972	0.758	0.001
black lm., Bronzone (5)	Zn	Pb	Cu	Ag	As	Sb	Tl	Mn	Mo	P	Na	K	Sr
Min.	2.443	4.956	< d.l.	< d.l.	1.060	0.186	0.186	351.533	374.449	20.481	2.733	5.700	5.700
Max.	140.789	4.454	6.699	< d.l.	77.066	3.174	1.624	518.350	1827.920	691.096	37.803	27.816	7.463
Average	116.988	3.410	5.781	-	27.640	1.667	0.747	357.370	857.525	496.089	29.593	13.911	6.324
Std deviation	23.415	0.730	0.643	-	27.796	0.892	0.588	100.298	583.966	116.886	7.320	9.811	0.703
d.l.	0.699	0.016	0.036	0.001	0.209	0.018	0.009	0.102	0.001	9.291	1.112	0.935	0.005
earthy lm., Bronzone (6)	Zn	Pb	Cu	Ag	As	Sb	Tl	Mn	Mo	P	Na	K	Sr
Min.	3.141	0.155	0.279	< d.l.	40.369	0.958	0.020	6.517	9.149	616.491	9.137	3.248	7.713
Max.	156.070	12.196	113.349	0.114	68.180	6.669	0.092	22.829	87.864	1160.967	35.626	53.413	17.635
Average	38.722	3.136	21.018	0.026	55.152	2.023	0.056	11.771	62.147	943.554	17.271	15.550	12.754
Std deviation	58.356	5.164	45.378	0.044	11.760	2.281	0.029	7.308	33.757	200.393	9.744	18.809	3.369
d.l.	0.606	0.024	0.052	0.001	0.197	0.028	0.001	0.288	0.001	8.022	1.003	0.758	0.001

1318 ppm) than that from Mt. Bronzone (average 15 ppm for both black limonite and earthy limonite). Na and K show a strong direct correlation (Figure 8a), suggesting that these elements may be present in minerals intermixed with the iron hydroxides (e.g., clay minerals). The limonite from the Como Lake-Valsassina area is more enriched in As and Tl (Figure 8b), as well as in Sb, Zn, Pb, Cu, Ag and Ti than that from Mt. Bronzone mines. Instead on the average the latter is more enriched in Ni, Mn and P if compared to the Como Lake-Valsassina area limonite. Black limonite is rich in Mn, while the earthy Mt. Bronzone limonite has Mn values comparable to those of the limonite from Gaeta and Pasturo (Figure 8c). Moreover, Mt. Bronzone black limonite has higher Mo concentrations than earthy limonite (Figure 8c), being similar to that of Gaeta limonite (average 850 and 1045 ppm, respectively). Limonite from the Gaeta mine has higher Pb and Zn concentrations compared to Mt. Bronzone limonitic ores (Figure 8d), this can be linked to the presence of Pb-Zn non-sulfides intermixed with the iron hydroxides (see the previous chapters). Instead, earthy limonite is more enriched in V and P (average 87 ppm V and 940 ppm P) than black limonite (average 18 ppm V and 495 ppm P) (Figure 8e).

In general, the two limonite types from Mt. Bronzone mines show different trace elements concentrations. This can be linked to different conditions during the supergene transformations of the ore and/or to different degrees of weathering, as well as to the weathering of different primary ore sources (pyrite for the black limonite and unknown for the earthy limonite).

DISCUSSIONS AND CONCLUSIONS

General considerations about the iron sulfides-rich deposits of the Lombard Alps

The Como Lake-Valsassina deposits have fine-grained Fe-Pb-Zn sulfides often with botryoidal textures mainly in their earlier ore stage. This ore characteristic may be linked to a fast deposition from a relatively supersaturated solution (Roedder, 1968; St. Marie and Kesler, 2000). These deposits may be linked to the precipitation from fluids characterized by a relatively high concentration and/or availability of H_2S, thus producing a larger degree of fluid supersaturation and finer-grained, more botryoidal textures (Roedder, 1968; St. Marie and Kesler, 2000). Pyrite was probably one of the main minerals in

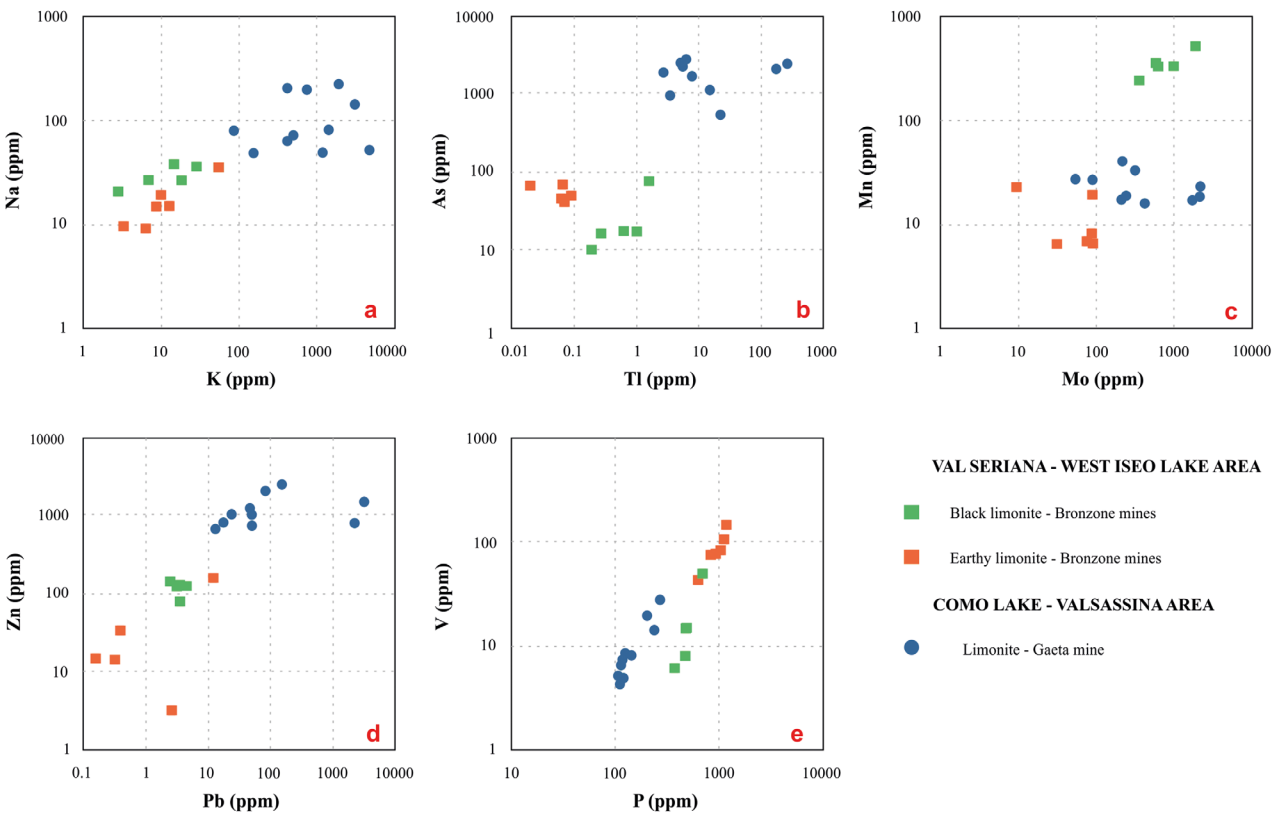

Figure 8. Trace element plots of Gaeta and Mt. Bronzone iron hydroxides: a) Na vs K; b) As vs Tl; c) Mn vs Mo; d) Zn vs Pb and f) V vs P.

the primary ore association in the Bronzone deposits, in fact iron hydroxides pseudomorphs on fine to coarse-grained massive pyrite (as cubic crystals, from 0.5 mm to 1.5 cm) are easily identifiable in the limonite masses. Mt. Bronzone pyrite shows much coarser grained textures than those of the Como Lake-Valsassina deposits: their ore precipitation may involve growth from a less saturated solution with fewer nuclei. Moreover, the Como Lake-Valsassina early ore stage shows colloidal marcasite and pyrite as dominant minerals, with less common pyritized microfossils and pyrite oolites and framboids. Possibly the latter are from the carbonate host rocks. However, it cannot be stated unequivocally that all the pyrite oolites are of sedimentary origin, in fact part of them can also be primary as suggested by Pufahl and Grimm (2003). Wilkin and Barnes (1997) report that the framboid formation could operate not only in marine and lacustrine waters but also with temperatures up to ~200°C, coherently with the occurrence of pyrite framboids in the paragenesis of metalliferous ore deposits (Wilkin and Barnes, 1997).

Generally, As concentration in pyrite is linked to the proportion of meteoric water to magmatic fluid within the system, with meteoric or basinal water abundances positively correlating with pyrite As concentrations (Li et al., 2021). In comparison, mineralizing fluids with higher abundance of magmatic fluid tend to form pyrite with higher concentrations of Co and lower concentrations of As (Rajabpour et al., 2017; Li et al., 2021). The pyrites from Gaeta and Mt. Bronzone plot close to the As apex in a Co-Ni-As diagram, indicating that this pyrite may have been formed from basinal fluids and/or meteoric water.

A brief discussion about the secondary non-sulfides minerals

All the studied deposits are characterized by the presence of pervasive iron hydroxides stockwork veinlets. These veins result, as well as a large part of the other gossan bodies, probably from the in-situ alteration of sulfides. In general, these veins do not seem to be linked to a limonite deposition caused by fluid migration into the host rock fractures during the weathering stage. This is suggested by the presence of fresh sulfides remains within these limonite veinlets in the Como Lake-Valsassina deposits and by the presence of iron hydroxides pseudomorphs on coarse grained pyrite in the Valseriana-West Iseo ones.

In a similar way, the oxidized Zn and Pb minerals in the gossan were formed mainly at the expense of the sulfides. All this suggests that the Zn-Pb-bearing solutions from the sulfides weathering were quickly neutralized by the local carbonate environment, and did not migrate over a long distance through the fractures of the host rock. Such a circulation is further confirmed by the co-occurrence of gypsum, whose formation generally takes place in supergene environments with limited fluid migration (Reichert and Borg, 2008).

Sulfates within the gossan, intermixed with iron hydroxides, are common in the Como Lake-Valsassina deposits. As previously discussed, the most common being gypsum, jarosite and fibroferrite. Fibroferrite is a secondary iron-bearing hydrous sulfate from pyrite weathering in an oxidizing environment (Alpers et al., 2001). Fibroferrite and other sulfates like jarosite, epsomite and gypsum are known to be typical products of acidic mine drainage (AMD) processes, according to local environmental conditions such as temperature, pH, relative humidity, oxygen and sulfate activity. The precipitation of iron sulfate minerals is caused by the evaporation of iron and sulfate rich acidic solutions in a superficial environment (Jerz and Rimstidt, 2003). Slight changes in temperature, humidity or other environmental conditions can negatively affect the stability of these sulfates and can lead to their dehydration, oxidation or dissolution. They are an intermediate step in the complex series of reactions leading to the precipitation of iron hydroxides starting from iron sulfides weathering (Jerz and Rimstidt, 2003).

Further considerations about the gossan ore are in the ESM.

Incorporation of trace elements into the sphalerite from Gaeta

Previous studies have shown that bivalent cations, such as Mn, Cd, Co and Fe, substitute Zn in the sphalerite lattice (e.g., Cook et al., 2009; Ye et al., 2011). Cook et al. (2012) and Belissont et al. (2014) fully support the incorporation of trivalent and tetravalent cations, such as Ga^{3+}, In^{3+} and probably Sn^{3+} or Sn^{4+}, via coupled substitutions, i.e., with monovalent cations as Cu and Ag.

A positive correlation was observed between Cu and Ga (Figure 6), supporting the coupled substitution $2Zn^{2+} \leftrightarrow Cu^{+}+Ga^{3+}$. The same principle applies to the coupled substitution of Cu and Sn replacing Zn in the sphalerite lattice (Figure 6), as expressed by the equation: $2Zn^{2+} \leftrightarrow Cu^{+}+Sn^{3+}$. In general, In is observed within the sphalerite lattice due coupled substitution ($2Zn^{2+} \leftrightarrow Cu^{+}+In^{3+}$) because Cu and In do not occur often in a divalent state in sulfides and sulfosalts. A positive In-Cu correlation can be seen in particular for early-stage Gaeta sphalerite. It is difficult to observe it in the other samples due to their higher concentrations of Cu (usually between 100 and 1000 ppm) compared to In (0.001-4 ppm) in most of the spots analyzed. The positive correlation between In and Sn (Figure 6) suggests a potentially coupled substitution $3Zn^{2+} \leftrightarrow In^{3+}+Sn^{3+}+\square$ (vacancy), which is reported also in previous studies (e.g., Belissont et al., 2014). There is also a steep positive correlation between Cu and Ge (and also between Cu and Ga+Ge) in all the analyzed sphalerite spots (Figure 6), suggesting the presence of a coupled

substitution. It can be inferred by the following equation: $2Cu^{+}+Ge^{4+}\leftrightarrow 3Zn^{2+}$ (Cook et al., 2009; Ye et al., 2011; Belissont et al., 2014). This substitution mechanism of Zn^{2+} by Ge^{2+} could suggest a reducing condition in the ore-forming fluids.

REE geochemistry of the iron sulfides

The Rare Earth Elements (REE) are hard cations (high charge/radius ratio) and they are characterized by broadly similar chemical behavior. Very small differences in their solubility occur because of the decrease of the ionic radii from light to heavy REE (e.g., Bau 1991; Migdisov et al., 2009).

REE are probably hosted in the fluid inclusions and crystal defects of pyrite and marcasite, due the difficult elemental substitution of Fe^{2+} by the REE. Thus, the REE are not controlled by the crystal structure of pyrite, and therefore they can be relied upon in order to investigate the characteristics of the ore-forming fluid (e.g., Gao et al., 2020).

Ho has a geochemical behavior similar to Y, although Ho is preferentially complexed and removed from fluids by Fe-oxides and organic particles. Seawater and seawater-derived fluids preserve super-chondritic (>28) Y/Ho values, while crustal fluids have lower chondritic Y/Ho values (Zhang et al. 1994; Nozaki et al. 1997; Bau and Dulski 1999; Gao et al., 2020).

As previously stated, pyrite and marcasite from the Como Lake-Valsassina deposits show a positive Eu anomaly compared to the PAAS. Ce is sensitive to redox conditions (Sholkovitz et al., 1994) and Eu is known to be more enriched in volcanic rocks if compared to sedimentary carbonates (Elderfield and Greaves, 1982). Generally hydrothermal fluids are characterized by positive Eu anomalies, mainly inherited by the dissolution of feldspars in igneous, volcanic or metamorphic rocks. Moreover, the incompatibility of Eu^{2+} in the crystal lattice of sulfides provides an opportunity to assess redox conditions and the temperature of fluids. Trivalent Eu shows higher enrichments at relatively low temperatures and it is sustained by reducing conditions during sulfide deposition (Bau and Möller, 1992; Li et al., 2020). The presence of a slightly positive Eu anomaly in Gaeta pyrite and marcasite may underlie the interaction between reducing hydrothermal fluids at a relatively low temperature, possibly basinal brines, and rocks of the metamorphic basement or volcano-clastic lenses within the carbonate rocks of the Triassic succession. Reducing condition during the sulfide deposition, for both Como Lake-Valsassina and Valseriana-West Iseo deposits, are underlined by the very low total REE contents of pyrite and marcasite, usually $\sum$REE<1 ppm (e.g., Xi et al., 2013; Yang et al., 2014). Finally, Gaeta pyrite and marcasite show Y/Ho ratios always <28, suggesting a precipitation from fluids of non-marine origin mainly.

Co/Ni ratios of pyrite and marcasite

Often displaying a similar geochemistry, Co and Ni are not discharged during pyrite recrystallization and they can be easily incorporated into its crystal lattice (e.g., Large et al., 2009; Koglin et al., 2010). Because of this, the Co/Ni ratio of pyrite is useful in discriminating pyrite of different origins (Price, 1972; Bralia et al., 1979). For example, the Co/Ni ratios in sedimentary pyrite are generally between 0.01 and 10 (Gregory et al., 2015). High Co and Ni concentrations and high Co/Ni ratios (~ Co/Ni>10) in pyrite may suggest an origin related to a high-temperature magmatic-hydrothermal regime (Bralia et al., 1979). Instead, pyrite linked to a sedimentary environment usually has low Co/Ni ratios (<1, Ni dominated).

The pyrite from Gaeta mine has low contents of Co and Ni (Ni<75 ppm and Co<11 ppm) with a Co/Ni ratio ranging from 0.02 to 5.60 (mean 0.58). It has Co-Ni contents and Co/Ni ratios comparable to those of sedimentary-related pyrite and MVT deposits, moreover these ratios partially overlap with the reference interval of SEDEX deposits (Figure 7). Gaeta marcasite shows Co/Ni ratios ranging from 0.008 and 0.07, comparable with those of sedimentary-related pyrite and partially overlapping the reference interval of MVT deposits (Figure 7). As previously discussed, hydrothermal pyrite exhibits Co/Ni ratios >1, however Co/Ni ratios similar to those of Gaeta pyrite were reported from various MVT deposits, e.g., Co/Ni mean value of 0.68 for the Hoshbulak Zn-Pb deposit at Xinjiang (China; Li et al., 2015) and Co/Ni ratios variable between 0.04-1.6, 0-0.70 and 0-0.69 from Qilinchang Pb-Zn deposit (China; Oyebamiji et al., 2020).

Mt. Bronzone pyrite shows Co/Ni ratios, ranging from 0.23 and 6.71 (mean 2.18), comparable with those of MVT deposits and with submarine hydrothermal vents-related deposits (Figure 7). This may suggest a hydrothermal origin for these iron deposits. (Figure 7).

Gaeta mine and Mt. Bronzone iron sulfides show Ni-Co contents and Co/Ni ratios far lower than IOCG and porphyry Cu deposits, suggesting the lack of hydrothermal fluids directly linked to magmatic activities.

Preliminary thermometric evaluations

The original sulfide assemblage of the iron-rich Pb-Zn gossan deposits of the Como Lake-Valsassina area include sphalerite in the mines of Gaeta, Piani d'Erna and Pasturo. The presence of sphalerite in the primary ore association is also suggested by hemimorphite and other Zn secondary minerals in the non-sulfide assemblages of other deposits. Sphalerite composition has been considered in order to distinguish among the different genetic conditions of

Table 5. GIMFis sphalerite geothermometer results. Sph-es: early-stage sphalerite, Sph-ls: late-stage sphalerite.

	Zn (Wt%)	Fe (Wt%)	Cd (ppm)	In (ppm)	Ga (ppm)	Ge (ppm)	Mn (ppm)	Zn/Cd	PC1	TEMP (±17.3 °C)
GAE: Sph-ls 1	60.86	1.23	35185.291	0.981	346.474	2.718	1.179	17.30	1.40	131.89
GAE: Sph-ls 2	61.67	1.26	26763.640	0.196	353.558	12.196	4.512	23.04	1.63	119.20
GAE: Sph-ls 3	62.87	1.22	13177.892	0.322	1926.177	435.456	0.988	47.71	3.05	41.89
GAE: Sph-ls 4	61.09	1.24	32459.711	3.792	560.912	7.182	1.509	18.82	1.52	125.57
GAE: Sph-ls 5	61.44	1.22	28749.715	3.052	753.685	259.287	0.642	21.37	2.57	68.18
GAE: Sph-ls 6	60.54	1.24	37956.431	1.635	595.800	3.800	1.094	15.95	1.55	123.94
GAE: Sph-ls 7	61.10	1.26	32003.062	1.751	742.416	2.575	2.587	19.09	1.32	136.03
GAE: Sph-ls 8	61.46	2.56	11351.428	< d.l.	4124.918	631.923	1.491	54.15	-	-
GAE: Sph-ls 9	62.76	1.31	15239.826	0.442	217.148	229.587	0.563	41.19	2.48	72.90
GAE: Sph-ls 10	63.42	1.40	6722.691	0.080	1319.500	84.189	1.735	94.35	2.60	66.71
GAE: Sph-ls 11	62.72	1.32	15446.746	0.986	360.434	233.508	0.606	40.61	2.49	72.33
GAE: Sph-es 1	64.03	1.39	1664.581	0.001	549.909	66.175	3.663	384.67	2.56	68.95
GAE: Sph-es 2	64.02	1.37	2123.064	< d.l.	399.230	17.075	0.702	301.55	-	-
GAE: Sph-es 3	62.92	1.71	10166.373	< d.l.	< d.l.	< d.l.	1.359	61.89	-	-
GAE: Sph-es 4	63.99	1.23	4280.998	< d.l.	0.180	< d.l.	0.745	149.48	-	-
GAE: Sph-es 5	64.10	1.17	3510.367	0.008	186.854	3.007	1.315	182.63	1.82	109.19
GAE: Sph-es 6	63.96	1.24	4210.466	0.018	115.631	0.935	1.151	151.93	1.36	133.79
GAE: Sph-es 7	64.08	1.27	2478.408	0.002	345.922	16.933	0.919	258.58	2.50	72.13
GAE: Sph-es 8	64.00	1.32	3148.776	< d.l.	64.075	4.078	1.061	203.26	-	-
GAE: Sph-es 9	64.11	1.27	2549.402	0.002	18.792	2.712	1.085	251.49	1.44	129.51
GAE: Sph-es 10	64.14	1.28	1604.320	< d.l.	492.554	35.311	2.039	399.85	-	-
GAE: Sph-es 11	63.92	1.38	3175.477	< d.l.	207.366	18.910	12.720	201.29	-	-
GAE: Sph-es 12	64.14	1.29	2059.084	< d.l.	39.573	2.285	0.502	311.54	-	-
GAE: Sph-es 13	60.24	1.25	1078.652	0.015	398.351	20.622	1.167	558.50	2.33	81.45
GAE: Sph-es 14	64.04	1.41	1915.121	0.001	23.050	1.896	16.598	334.40	0.93	157.50
GAE: Sph-es 15	64.01	1.44	1520.228	< d.l.	348.437	64.354	2.696	421.10	-	-
GAE: Sph-es 16	63.89	1.57	1625.293	0.005	97.793	44.370	0.950	393.15	2.27	84.50
GAE: Sph-es 17	63.04	1.51	10737.932	0.016	184.188	9.263	1.450	58.71	1.86	106.76
GAE: Sph-es 18	63.68	1.74	1795.596	0.003	367.447	18.591	6.747	354.67	2.00	99.14
GAE: Sph-es 19	61.72	1.79	1244.695	0.001	39.287	20.606	6.598	495.92	1.66	117.74
GAE: Sph-es 20	63.92	1.51	1946.616	0.013	127.118	8.967	1.376	328.39	1.80	109.81
GAE: Sph-es 21	63.92	1.53	1924.573	0.005	9.400	23.997	0.722	332.14	1.68	116.72
GAE: Sph-es 22	63.91	1.54	1901.630	0.005	12.303	5.026	3.635	336.10	1.08	149.41

the deposit (e.g., Schwartz, 2000; Wen et al., 2016), or for tracking changes in ore/fluid interaction in an ore deposit (e.g., Gottesmann and Kampe, 2007; Gottesmann et al., 2009). According to Wen et al. (2016), the Zn/Cd ratio of sphalerite can allow us to distinguish among high temperature (skarn, porphyry), low temperature (Mississippi Valley Type) and exhalative deposit types, which are characterized by specific ranges. Gaeta late-stage sphalerite has Zn/Cd ratios between 17 and 95 with Cd values ranging from 6723 to 35185 ppm, while the Zn/Cd ratios range between 60 and 560 for early-stage sphalerite (Table 5). According to the protocol proposed by Wen et al. (2016), the relatively constrained late-stage sphalerite Zn/Cd ratios overlap the reference intervals proposed by the authors for low-temperature (<200 °C) MVT and carbonate-hosted veins. On the other hand, early-stage sphalerite shows more variable Zn/Cd ratios, overlapping both the reference intervals suggested for low-

temperature and sedimentary exhalative mineralization. All this is coherent with the previous discussion about Co/Ni rations in Gaeta pyrite and marcasite.

The variability of the sphalerite composition, in terms of major, minor and trace elements has been used for thermometric evaluations (e.g., Kullerud, 1953) and, recently, a sphalerite geothermometer was proposed by Frenzel et al. (2016). I tried to apply the GIMFis geothermometer of Frenzel et al. (2016) in this paper. This method is based on the statistical evaluation, by means of the main component analysis, of a large dataset of sphalerite compositions from a large number of ore deposits worldwide, correlating them with the homogenization temperatures of fluid inclusions. The sphalerite geothermometer is based on its Ga, Ge, In, Mn and Fe contents. Table 5 shows the estimated temperatures obtained for the Gaeta orebody. Its temperatures show average values of 110 °C and 93 °C (±17.3 °C) for early and late-stage sphalerite respectively.

Possible evidence about the deposits genesis

As it was already suggested, the ore deposits in the Como Lake-Valsassina area have a probable epigenetic origin. Ixer (2006) suggested a probable origin from a primary Fe-Pb-Zn-Ba sulfide-rich ore body for the Piani d'Erna deposits, linked to the Pb-Zn-Alpine-type deposits hosted by the Ladinian-Carnian boundary-related breccias at the top of the Esino platform. In a similar way Curioni (1842) and Repossi (1904) suggested an epigenetic origin for the Gaeta cape deposit, linked to the migration of metals-rich fluids along heavily fractured parts of the Esino Formation.

The field and petrographic data presented in this paper point out that the iron sulfides-rich deposits of the Como Lake-Valsassina area result from the weathering of Fe-Pb-Zn (As, Sb, Ag) massive sulfides barite/carbonate-hosted deposits. Moreover, the high Sb, As and Cd concentrations in the sulfide assemblages agree with a hydrothermal fluid circulation through volcaniclastic sediments (e.g., Mondillo et al., 2020), as suggested also by the Eu positive anomalies of Gaeta iron sulfides. The probable metal source is the Triassic sedimentary basin, with metal leaching from limestones that host also minor volcanoclastic bodies, arenaceous conglomerates (e.g., Bellano Fm.) and the underlying Permian-basement rocks.

The geometries of the orebodies, hosted by E-W, NW-SE and N–S-striking faults, by paleo-karst cavities and by dissolution/collapse breccias, confirm the hypothesis of an epigenetic origin for the original primary sulfides. An epigenetic origin of the ore is suggested also by its abundance of Sb-As-Ag sulfosalts: they were observed by petrographic observations and hypothesized according to the pyrite, marcasite and sphalerite trace element data. These features are characteristic also of MVT and Pb-Zn Alpine-type deposits.

These Fe-Pb-Zn deposits seem to show a spatial relationship with the Alpine-type deposits in the same area. A relationship that seems confirmed by the geochemical data of sphalerite, pyrite and marcasite. The first to hypothesize a genetic link between the Alpine-type deposits in the Valsassina-Lario area and the iron-gossan deposits was Ixer (2006). However, having only petrographic observations and limited geochemical analyses of the Piani d'Erna deposit, it was not possible for him to prove it. The data collected agree with Ixer's hypothesis and they seem to demonstrate a possible genetic link between the iron sulfides-rich deposits and the Alpine-type deposits of the same area. The genesis of these deposits seems to be linked to the migration of Fe-Pb-Zn-Ba-rich reducing basinal fluids that leaked along strongly fractured parts of the Esino Fm., with a possible genetic-link with Resinelli Pb-Zn-Fe-Ba Alpine-type deposits.

The features of Como Lake-Valsassina deposits can be resumed as: a) stratabound epigenetic Fe-Pb-Zn-Ba (As-Sb-Ag) deposits within the Esino limestone, showing geometries typical of MVT and Pb-Zn Alpine-type deposits; b) ore precipitation from reducing non-marine-derived fluids, possibly basinal-brines; c) Co/Ni ratios typical of sedimentary pyrite and some MVT deposits; d) sphalerite Zn/Cd ratios typical of MVT and SEDEX deposits; and e) relatively-low temperature deposits (GIMFis sphalerite geothermometer).

The Lombard Zn-Pb Alpine-type deposits occur in the CMB Fm., within the black shales of the 'Basal Tongue' of the Gorno Fm., in the limestones of the Breno Fm. and finally in the upper portion of Esino Fm. (Omenetto, 1966; Rodeghiero et al., 1986; Mondillo et al., 2019). This stratigraphic interval is generally known as 'Metallifero' (e.g. Omenetto, 1966). According to the new data reported in this paper, the lower limit of 'Metallifero' could be extended in order to comprise the whole Esino Fm. in western Lombardy.

Esino and Breno limestones were affected by a multiphase dolomitization, with at least three main dolomite generations (D1, D2, and D3; Hou et al., 2016). D1 dolomite formation is probably linked to shallow burial settings (temperature around 45-50 °C). D2 and D3 dolomites formed at a later stage under mid-to deeper burial settings at higher temperatures (around 110 °C) from dolomitizing hot basinal fluids, possibly hydrothermal, characterized by a higher salinity with also a possible contribution from volcanic-related fluids (basinal fluids circulated in volcaniclastics sediments; Hou et al., 2016). The Como Lake-Valsassina deposits are associated with the dolomitized portions of Esino Limestone, characterized

by fine to coarse grained dolomite and dolomite coarse veinlets (D2-D3). Moreover, the temperature estimates obtained from the GIMFis sphalerite geothermometer are very similar to those of the dolomitizing fluids of D2 and D3. The Gaeta iron sulfides, as previously discussed, precipitated from basinal fluids that possibly circulated in volcaniclastics sediments or basement rocks, as described by Hou et al. (2016) for Esino and Breno multiphase dolomitization. Because of this, it is possible to hypothesize that the hydrothermal event that generated the Como Lake-Valsassina deposits can be linked to the multiphase dolomitization that affected Esino and Breno limestones, coherently with the genetic models of MVT and Zn-Pb Alpine-type deposits.

The deposits discussed in this paper show Fe-enrichments that are unusual in the Alpine-type deposits of the Lombard Alps. St. Marie et al. (2001) reported MVT deposits where iron is significantly more abundant than lead and zinc in high-temperature (>200 °C), relatively acidic brines with low sulfur contents. Instead, zinc dominates under most of the other conditions, high temperature and high sulfur content brines included. This evidence suggests that iron-rich Mississippi Valley–type deposits formed from brines expelled from the deepest, hottest parts of sedimentary basins. The presence of fine-grained colloidal ore in the Como Lake-Valsassina deposits may suggest an ore precipitation from fluids characterized by relatively high concentration and/or availability of H_2S. Moreover, the GIMFis geothermometer of Frenzel et al. (2016) shows temperature estimates always below 200 °C for early and late-stage sphalerite. Taking into consideration these two facts, it is clear that the Como Lake-Valsassina deposits exhibit features not coherent with those of Fe-rich MVT deposits. Another hypothesis about the unusual Fe-enrichment in these deposits may be a leaching from the iron-rich paleo-soils levels linked to emersion events of the Esino Fm. Bahamian carbonate platform.

The almost total absence of non-weathered sulfides in the deposits of the Val Seriana-West Iseo Lake area makes their genetic interpretation more difficult. These deposits might be linked to the circulation of iron-rich basinal and/or meteoric-derivate (low temperature?) hydrothermal fluids, as suggested by the As concentrations and the Co/Ni ratios of pyrite. A possible iron source may be represented by sin-sedimentary iron-enrichments within the Late Triassic sedimentary basin. The Albenza and Sedrina formations are over the mixed shale-carbonate succession of the Zu Limestone (Figure1), interested by iron-enrichments as iron-oxide crusts, iron-rich tempestites and Fe-rich hardgrounds (Galli et al., 2007). Leaving these speculations aside, our data do not allow us to establish a clear genetic model for the Val Seriana-West Iseo deposits, because of the almost total primary ore weathering and of the consequent lack of samples suitable for more detailed analyses and petrographic studies. The ore paragenesis of these deposits is almost unknown due the total supergene transformation of the primary ore, since only the presence of (rare) pyrite relics were detected.

ACKNOWLEDGMENTS

The Author is grateful to Prof. Marco Tizzoni (Chercheur associé CNRS IRAMAT, Université de Technologie Belfort-Montbéliard, Belfort-Cedex, France) who reviewed this paper and financially supported the ICP-LA-MS analyses. The author is also grateful to Mr. Luca Brevi, the rediscoverer of the old mining sites of Mt. Bronzone and to Dr. Paolo Gentile (Piattaforma Interdipartimentale di Microscopia, Università di Milano Bicocca, Milan, Italy) for his support during polished sample preparations and the SEM-EDS observations and analyses.

REFERENCES

Bau M., 1991. Rare-earth element mobility during hydrothermal and metamorphic fluid-rock interaction and the significance of the oxidation state of europium. Chemical Geology 93, 219-230.

Bau M. and Dulski P., 1996. Anthropogenic origin of positive gadolinium anomalies in river waters. Earth and Planetary Science Letters 143, 245-256.

Belissont R., Boiron M.C., Luais B., Cathelineau M., 2014. LA-ICPMS analyses of minor and trace elements and bulk Ge isotopes in zoned Ge-rich sphalerites from the Noailhac–Saint-Salvy deposit (France): Insights into incorporation mechanisms and ore deposition processes. Geochimica et Cosmochimica Acta 126, 518-540.

Berner Z.A., Puchelt H., Nöltner T., Kramar U., 2013. Pyrite geochemistry in the Toarcian Posidonia Shale of south-west Germany: Evidence for contrasting trace-element patterns of diagenetic and syngenetic pyrites. Sedimentology 60, 548-573.

Berra F. and Felletti F., 2011. Syndepositional tectonics recorded by soft-sediment deformation and liquefaction structures (continental Lower Permian sediments, Southern Alps, Northern Italy): stratigraphic significance. Sedimentary Geology 235, 249-263.

Berra F., 2012. Sea-level fall, carbonate production, rainy days: how do they relate? Insight from Triassic carbonate platforms (Western Tethys, Southern Alps, Italy). Geology 40, 271-274.

Berra F. and Carminati E., 2012. Differential compaction and early rock fracturing in high-relief carbonate platforms: numerical modelling of a Triassic case study (Esino Limestone, Central Southern Alps, Italy). Basin Research 24, 598-614.

Bersezio R., Jadoul F., Chinaglia N., 1997. Geological map of

the Norian-Jurassic succession of the Southern Alps north of Bergamo. An explanatory note. Bollettino della Società Geologica Italiana 116, 363-378.

Chace F.M., 1956. Abbreviations in field and mine geological mapping. Economic Geology 51, 712-723.

Curioni G., 1842. Su la giacitura, l'estrazione e il trattamento dei minerali di ferro in Lombardia. Hoepli, Milano, 16 pp.

Curioni G., 1877. Geologia applicata delle provincie lombarde. Hoepli, Milano, 418 pp.

Elderfield H. and Greaves M.J., 1982. The rare earth elements in seawater. Nature 296, 214-219.

Frenzel M., Hirsch T., Gutzmer J., 2016. Gallium, germanium, indium and other trace and minor elements in sphalerite as a function of deposit type – a meta-analysis. Ore Geology Reviews 52-78.

Gadd M.G., Layton-Matthews D., Peter J.M., 2016. Non-hydrothermal origin of apatite in SEDEX mineralization and host rocks of the Howard's Pass district, Yukon, Canada. American Mineralogist 101, 1061-1071.

Galli M.T., Jadoul F., Bernasconi S.M., Cirilli S., Weissert H., 2007. Stratigraphy and palaeoenvironmental analysis of the Triassic–Jurassic transition in the western Southern Alps (Northern Italy). Palaeogeography, Palaeoclimatology, Palaeoecology 244, 52-70.

Gao B., Zhang L., Jin X., Li W., Bai Y., Sakyi P.A., 2020. Re-Os geochronology and trace element characteristics of the hydrothermally reworked pyrite of the Gaobanhe sediment-hosted polymetal pyrite deposit in Northern China and its geological significance. Journal of Geochemical Exploration 215.

Gottesmann W. and Kampe A., 2007. Zn/Cd ratios in calcsilicate-hosted sphalerite ores at Tumurtijn-ovoo, Mongolia. Chemie der Erde - Geochemistry 67, 323-328.

Gottesmann W., Gottesmann B., Seifert W., 2009. Sphalerite composition and ore genesis at the Tumurtjin-ovoo Fe–Mn–Zn skarn deposit, Mongolia. Neues Jahrbuch für Mineralogie, Abhandlungen 185, 249-280.

Gregory D.D., Large R.R., Halpin J.A., Baturina E.L., Lyons T.W., Wu S., Danyushevsky L., Sack P.J., Chappaz A., Maslennikov V.V., Bull S.W., 2015. Trace Element Content of Sedimentary Pyrite in Black Shales. Economic Geology 110, 1389-1410.

Hou Y., Azmy K., Berra F., Jadoul F., Blamey N.J.F., Gleeson S.A., Brand U., 2016. Origin of the Breno and Esino dolomites in the western Southern Alps (Italy): Implications for a volcanic influence. Marine and Petroleum Geology 69, 38-52.

Ixer R.A., 2006. The mineralogy of gossans and base metal-baryte ores present at the Late Iron Age mine and smelting site. In: Alle Origini della Siderurgia Lecchese. Ricerche archeometallurgiche ai Piani d'Erna. (Eds.) Tizzoni M., Cucini C., Ruffa M., Civici Musei di Lecco, Lecco, Italy, 27-31.

Jadoul F., Gervasutti M., Fantini Sestini N., 1992. The middle triassic of the Brembana Valley: preliminary study of the esino platform (Bergamasc Alps). Rivista Italiana di Paleontologia e Stratigrafia 98, 299-324.

Jadoul F. and Galli M.T., 2008. The Hettangian shallow water carbonates after the Triassic/Jurassic biocalcification crisis. Rivista Italiana di Paleontologia e Stratigrafia 114, 453-470.

Jadoul F. and Omenetto P., 1980. Diagenetic evolution of ore-bearing sediments in karst cavities: examples from the Triassic of the Bergamasc Alps (Gorno District, Northern Italy). N f J Geol Paläont 1, 17-32

Jervis G., 1873. I tesori sotterranei dell'Italia. Loescher, Torino, 348 pp.

Jerz J.K. and Rimstidt J.D., 2003. Efflorescent iron sulfate minerals: paragenesis, relative stability, and environmental impact. American Mineralogist 88, 1019-1032.

Keith M., Häckel F., Haase K.M., Schwarz-Schampera U., Klemd R., 2016. Trace element systematics of pyrite from submarine hydrothermal vents. Ore Geology Reviews 72, 728-745.

Koglin N., Frimmel H.F., Lawrie Minter W.E., Brätz H., 2010. Trace-element characteristics of different pyrite types in Mesoarchean to Paleoproterozoic placer deposits. Mineralium Deposita 45, 259-280.

Kullerud G., 1953. The FeS-ZnS system; a geological thermometer. Norsk geologisk Tidsskrift 32, 61-147.

Large R.R., Danyushevsky L., Hollit C., Maslennikov V., Meffre S., Gilbert S., Bull S., Scott R., Emsbo P., Thomas H., Singh B., Foster J., 2009. Gold and trace element zonation in pyrite using a laser imaging technique: implications for the timing of gold in orogenic and Carlin-style sediment-hosted deposits. Economic Geology 104, 635-668.

Large R.R., Halpin J.A., Danyushevsky L.V., Maslennikov V.V., Bull S.W., Long J.A., Gregory D., Lounejeva E., Lyons T.W., Sack P., McGoldrick P., Calver C.R., 2014. Trace element content of sedimentary pyrite as a new proxy for deep-time ocean–atmosphere evolution. Earth and Planetary Science Letters 389, 209-220.

Laubscher H.P., 1985. Large scale thin-skin thrusting in the Southern Alps: kinematic models. Geological Society of America Bulletin 96, 710-718.

Li Z.D., Xue C.J., Wu Y., Dong X.F., Wang S.C., Yu R.A., and Chen J.Q., 2015. The nappe-hosted Hoshbulak MVT Zn-Pb deposit, Xinjiang, China: A review of the geological, elemental and stable isotopic constraints. Ore Geology Reviews 70, 47-60.

Li H., Palinkaš L.A., Evans N.J., Watanabe K., 2020. Genesis of the Huangshaping W-Mo–Cu–Pb–Zn deposit, South China: role of magmatic water, metasomatized fluids, and basinal brines during intra-continental extension. Geological Journal 10, 1-22.

Li X.H., Bai L.A., Yue Z.H., Pang B.C., Wei D.T., 2021. Mineralization processes involved in the formation of

the Jinya Carlin-type Au deposit, northwestern Guangxi, China: evidence from in situ trace element and S isotope geochemistry of Au-bearing zoned pyrite. Ore Geology Reviews 138, 104376.

Longerich H.P., Jackson S.E., Gunther D., 1996. Laser ablation inductively coupled plasma mass spectrometric transient signal data acquisition and analyte concentration calculation. Journal of Analytical Atomic Spectrometry 11, 899-904.

Migdisov A.A., Williams-Jones A.E., Wagner T., 2009. An experimental study of the solubility and speciation of the Rare Earth Elements (III) in fluoride- and chloride-bearing aqueous solutions at temperatures up to 300 °C. Geochimica et Cosmochimica Acta 73, 7087-7109.

Mondillo N., Boni M., Lupone F., Joachimski M., Balassone G., De Angelis M., Zanin S., 2019. The Gorno Zn project (Bergamo, Italy): mineralogy, isotopic characterization and genesis of the "oxide-type" ores. Geophysical Research Abstracts 21, 1-11.

Mondillo N., Lupone F., Boni M., Joachimski M., Balassone G., De Angelis M., Zanin S., Granitzio F., 2020. From Alpine-type sulfides to nonsulfides in the Gorno Zn project (Bergamo, Italy). Mineralium Deposita 55, 953-970.

Mukherjee I. and Large R.R., 2017. Application of pyrite trace element chemistry to exploration for SEDEX Style Zn–Pb deposits: McArthur Basin, Northern Territory, Australia. Ore Geology Reviews 81, 1249-1270.

Nozaki Y., Zhang J., Amakawa H., 1997. The fractionation between Y and Ho in the marine environment. Earth and Planetary Science Letters 148, 329-340.

Omenetto P., 1966. Il giacimento piombo-zincifero di Oltre il Colle (Alpi Bergamasche). Memorie dell'Istituto Geologico della R. Università di Padova 25, 3-49.

Oyebamiji A., Hu R., Zhao C., Zafar T., 2020. Origin of the Triassic Qilinchang Pb-Zn deposit in the western Yangtze block, SW China: insights from in-situ trace elemental compositions of base metal sulphides. Journal of Asian Earth Sciences 192, 104292.

Palme H. and O'Neill H., 2014. Cosmochemical Estimates of Mantle Composition. Planets, Asteriods, Comets and The Solar System, Volume 2 of Treatise on Geochemistry (Second Edition). Elsevier, 149-211.

Price B.G., 1972. Minor elements in pyrites from the Smithers Map area, B.C. and exploration applications of minor elements studies. Thesis Univ. of British Columbia, 270 pp.

Pufahl P.K. and Grimm K.A., 2003. Coated phosphate grains: proxy for physical, chemical, and ecological changes in seawater. Geology 31, 801-804.

Rajabpour S., Behzadi M., Jiang S.Y., Rasa I., Lehmann B., Ma Y., 2017. Sulfide chemistry and sulfur isotope characteristics of the Cenozoic volcanic-hosted Kuh-Pang copper deposit, Saveh county, northwestern central Iran. Ore Geology Reviews 86, 563-583.

Reichert J. and Borg G., 2008. Numerical simulation and a geochemical model of supergene carbonate-hosted non-sulphide zinc deposits. Ore Geology Reviews 33, 134-151.

Repossi E., 1904. Su alcuni minerali della Gaeta (Lago di Como). Atti Società Italiana di Scienze Naturali 43, 423-436.

Rodeghiero F., Jadoul F., Vailati G., Venerandi I., 1986. Dati preliminari sulle mineralizzazioni a Pb–Zn dell'area tra Mandello e Ballabio. Memorie della Società Geologica Italiana 32, 133-150.

Roedder E., 1968. The noncolloidal origin of colloform textures in sphalerite. Economic Geology 63, 451-471.

Ronchi P., Jadoul F., Ceriani A., Di Giulio A., Scotti P., Ortenzi A., Previde Massara E., 2011. Multistage dolomitization and distribution of dolomitized bodies in Early Jurassic carbonate platforms (Southern Alps, Italy). Sedimentology 58, 352-365.

Schmid S.M., Aebli H.R., Heller F., Zingg A., 1989. The role of the periadriatic line in the tectonic evolution of the Alps. In: Coward M.P., Dietrich D., Park R.G. (Eds.), Alpine tectonics 45, 153-171.

Schumacher M.E., Schönborn G., Bernoulli D., Laubscher H., 1997. Rifting and collision in the Southern Alps. In: Deep Structure of the Swiss Alps: Results from the National Research Program 20 (NRP 20), Pfiffner O. A., Lehner P., Heitzmann P., Mueller S., Steck A. (Eds.), Birkhäuser, Basel, Switzerland, 186-204.

Schwartz M.O., 2000. Cadmium in zinc deposits: economic geology of a polluting element. International Geology Review 42, 445-469.

Sciunnach D., Garzanti E., Confalonieri M., 1996. Stratigraphy and petrography of Upper Permian to Anisian terrigenous wedges (Verrucano Lombardo, Servino and Bellano Formations; western Southern Alps). Rivista Italiana di Paleontologia e Stratigrafia 102, 27-48.

Sholkovitz E.R., Landing W.M., Lewis B.L., 1994. Ocean particle chemistry: The fractionation of rare earth elements between suspended particles and seawater. Geochimica et Cosmochimica Acta 58, 1567-1579.

St. Marie J., Kesler S.E., Allen C.R., 2001. Origin of iron-rich Mississippi Valley-type deposits. Geology 29, 59-62.

Taylor S.R. and MacLennan S.M., 2009. Planetary Crusts: Their Composition, Origin and Evolution. Cambridge University Press, London, 378 pp.

Tizzoni M., 1998. Il comprensorio minerario e metallurgico valsassinese. Monografie Musei Civici di Lecco, Lecco, 447 pp.

Tizzoni M., Cucini C., Ruffa M., 2006. Ricerche archeo-metallurgiche ai Piani d'Erna. Musei Civici di Lecco, Lecco, 188 pp.

Vola G. and Jadoul F., 2014. Applied stratigraphy and carbonate petrography of the Arabescato Orobico dimension stone from the Bergamasc Alps (Calcare Rosso, Italy). Italian Journal of Geosciences 133, 294-314.

Wang C., Yang L., Bagas L., Evans N.J., Chen J., Du B., 2018. Mineralization processes at the giant Jinding Zn–Pb deposit,

Lanping Basin, Sanjiang Tethys Orogen: evidence from in situ trace element analysis of pyrite and marcasite. Geological Journal 53, 1279-1294.

Wen H.J., Zhu C.W., Zhang Y.X., Cloquet C., Fan H.F., Fu S.H., 2016. Zn/Cd ratios and cadmium isotope evidence for the classification of lead-zinc deposits. Sci. Reports, 6, 25273.

Wilkin R.T. and Barnes H.L., 1997. Formation processes of framboidal pyrite. Geochimica et Cosmochimica Acta 61, 323-339.

Ye L., Cook N.J., Ciobanu C.L., Liu Y.P., Zhang Q., Liu T.G., Gao W., Yang Y.L., Danyushevskiy L., 2011. Trace and minor elements in sphalerite from base metal deposits in South China: a LA-ICPMS study. Ore Geology Reviews 39, 188-217.

Zanchetta S., Malusà M.G., Zanchi A., 2015. Precollisional development and Cenozoic evolution of the Southalpine retrobelt (European Alps). Lithosphere 7, 662-681.

Zhang J., Amakawa H., Nozaki Y., 1994. The comparative behaviors of yttrium and lanthanides in the seawater of the north Pacific. Geophysical Research Letters 21, 2677-2680.